EUROPEAN ORGANIZATION FOR NUCLEAR RESEARCH

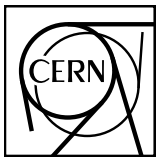

ALICE-ANA-2016-xxx
December 6, 2016

Lambda-Kaon and Cascade-Kaon Femtoscopy in Pb-Pb Collisions at $\sqrt{s_{NN}} = 2.76$ TeV from the LHC ALICE Experiment

Jesse T. Buxton[1]

1. Department of Physics, The Ohio State University, Columbus, Ohio, USA

Email: jesse.thomas.buxton@cern.ch

Abstract

We present results from a femtoscopic analysis of Lambda-Kaon correlations in Pb-Pb collisions at $\sqrt{s_{NN}}$ = 2.76 TeV by the ALICE experiment at the LHC. All pair combinations of Λ and $\bar{\Lambda}$ with K^+, K^- and K^0_S are analyzed. The femtoscopic correlations are the result of strong final-state interactions, and are fit with a parametrization based on a model by R. Lednicky and V. L. Lyuboshitz [1]. This allows us to both characterize the emission source and measure the scattering parameters for the particle pairs. We observe a large difference in the Λ-K^+ ($\bar{\Lambda}$-K^-) and Λ-K^- ($\bar{\Lambda}$-K^+) correlations in pairs with low relative momenta ($k^* \lesssim 100$ MeV). Additionally, the average of the Λ-K^+ ($\bar{\Lambda}$-K^-) and Λ-K^- ($\bar{\Lambda}$-K^+) correlation functions is consistent with our Λ-K^0_S ($\bar{\Lambda}$-K^0_S) measurement. The results suggest an effect arising from different quark-antiquark interactions in the pairs, i.e. $s\bar{s}$ in Λ-K^+ ($\bar{\Lambda}$-K^-) and $u\bar{u}$ in Λ-K^- ($\bar{\Lambda}$-K^+). To gain further insight into this hypothesis, we currently are conducting a Ξ-K femtoscopic analysis.

Contents

List of Figures

1 Introduction

NOTE: An updated version of this analysis note should be uploaded before 9 December 2016. Amongst other additions, this new version will include an estimate for my systematic errors both in the correlation function data points, and in the extracted fit parameters.

We present results from a femtoscopic analysis of Lambda-Kaon correlations in Pb-Pb collisions at $\sqrt{s_{NN}}$ = 2.76 TeV by the ALICE experiment at the LHC. All pair combinations of Λ and $\bar{\Lambda}$ with K^+, K^- and K^0_S are analyzed. The femtoscopic correlations are the result of strong final-state interactions, and are fit with a parametrization based on a model by R. Lednicky and V. L. Lyuboshitz [1]. This allows us to both characterize the emission source and measure the scattering parameters for the particle pairs. We observe a large difference in the Λ-K^+ ($\bar{\Lambda}$-K^-) and Λ-K^- ($\bar{\Lambda}$-K^+) correlations in pairs with low relative momenta ($k^* \lesssim 100$ MeV). Additionally, the average of the Λ-K^+ ($\bar{\Lambda}$-K^-) and Λ-K^- ($\bar{\Lambda}$-K^+) correlation functions is consistent with our Λ-K^0_S ($\bar{\Lambda}$-K^0_S) measurement. The results suggest an effect arising from different quark-antiquark interactions in the pairs, i.e. $s\bar{s}$ in Λ-K^+ ($\bar{\Lambda}$-K^-) and $u\bar{u}$ in Λ-K^- ($\bar{\Lambda}$-K^+). To gain further insight into this hypothesis, we currently are conducting a Ξ-K femtoscopic analysis.

2 Data Sample and Software

2.1 Data Sample

The analysis used "pass 2" reconstructed Pb-Pb data from LHC11h (AOD145). The runlist was selected from runs with global quality tag "1" in the ALICE Run Condition Table. Approximately 40 million combined central, semi-central, and minimum bias events were analyzed. Runs from both positive (++) and negative (--) magnetic field polarity settings were used.

Run list: 170593, 170572, 170388, 170387, 170315, 170313, 170312, 170311, 170309, 170308, 170306, 170270, 170269, 170268, 170230, 170228, 170207, 170204, 170203, 170193, 170163, 170159, 170155, 170091, 170089, 170088, 170085, 170084, 170083, 170081, 170040, 170027, 169965, 169923, 169859, 169858, 169855, 169846, 169838, 169837, 169835, 169591, 169590, 169588, 169587, 169586, 169557, 169555, 169554, 169553, 169550, 169515, 169512, 169506, 169504, 169498, 169475, 169420, 169419, 169418, 169417, 169415, 169411, 169238, 169167, 169160, 169156, 169148, 169145, 169144, 169138, 169099, 169094, 169091, 169045, 169044, 169040, 169035, 168992, 168988, 168826, 168777, 168514, 168512, 168511, 168467, 168464, 168460, 168458, 168362, 168361, 168342, 168341, 168325, 168322, 168311, 168310, 168115, 168108, 168107, 168105, 168076, 168069, 167988, 167987, 167985, 167920, 167915

Analysis was also performed on the LHC12a17a_fix (AOD149) Monte Carlo HIJING events for certain checks. THERMINATOR2 was also used for certain aspects, such as transform matrices described feed-down contributions.

2.2 Software

The analysis was performed on the PWGCF analysis train using AliRoot v5-08-18-1 and AliPhysics vAN-20161027-1.

The main classes utilized include: AliFemtoVertexMultAnalysis, AliFemtoEventCutEstimators, AliFemtoESDTrackCutNSigmaFilter, AliFemtoV0TrackCutNSigmaFilter, AliFemtoXiTrackCut, AliFemtoV0PairCut, AliFemtoV0TrackPairCut, AliFemtoXiTrackPairCut, and AliFemtoAnalysisLambdaKaon. All of these classes are contained in /AliPhysics/PWGCF/FEMTOSCOPY/AliFemto and .../AliFemtoUser.

3 Data Selection

3.1 Event Selection and Mixing

The events used in this study were selected with the class AliFemtoEventCutEstimators according to the following criteria:

- Triggers
  - minimum bias (kMB)
  - central (kCentral)
  - semi-central (kSemiCentral)
- z-position of reconstructed event vertex must be within 10 cm of the center of the ALICE detector
- the event must contain at least one particle of each type from the pair of interest

The event mixing was handled by the AliFemtoVertexMultAnalysis class, which only mixes events with like vertex position and centrality. The following criteria were used for event mixing:

- Number of events to mix = 5
- Vertex position bin width = 2 cm
- Centrality bin width = 5

The AliFemtoEventReaderAODChain class is used to read the events. Event flatteneing is not currently used. FilterBit(7). The centrality is determined by the "V0M" method of AliCentrality, set by calling AliFemtoEventReaderAOD::SetUseMultiplicity(kCentrality). I utilize the SetPrimaryVertexCorrectionTPCPoints switch, which causes the reader to shift all TPC points to be relative to the event vertex.

3.2 $K^{\pm}$ Track Selection

Charged kaons are identified using the AliFemtoESDTrackCutNSigmaFilter class. The specific cuts used in this analysis are as follows:

Track Selection:

- Kinematic range:
  - $0.14 < p_T < 1.5$
  - $|\eta| < 0.8$
- FilterBit(7)
  - TPC tracks
- Track Quality
  - Minimum number of clusters in the TPC (fminTPCncls) = 80
  - Maximum allowed χ^2/N_{DOF} for ITS clusters = 3.0
  - Maximum allowed χ^2/N_{DOF} for TPC clusters = 4.0
- Primary Particle Selection:

    - Maximum XY impact parameter = 2.4
    - Maximum Z impact parameter = 3.0
  - Remove particles with any kink labels (fRemoveKinks = true)
  - Maximum allowed sigma to primary vertex (fMaxSigmaToVertex) = 3.0

$K^{\pm}$ Identification:

  - PID Probabilities:
    - K: > 0.2
    - π: < 0.1
    - μ: < 0.8
    - p: < 0.1
  - Most probable particle type must be Kaon (fMostProbable=3)
  - TPC and TOF N_{σ} cuts:
    - p < 0.4 GeV/c: $N_{\sigma K,TPC} < 2$
    - $0.4 <$ p < 0.45 GeV/c: $N_{\sigma K,TPC} < 1$
    - $0.45 <$ p < 0.8 GeV/c: $N_{\sigma K,TPC} < 3$ & $N_{\sigma K,TOF} < 2$
    - $0.8 <$ p < 1.0 GeV/c: $N_{\sigma K,TPC} < 3$ & $N_{\sigma K,TOF} < 1.5$
    - p > 1.0 GeV/c: $N_{\sigma K,TPC} < 3$ & $N_{\sigma K,TOF} < 1$
  - Electron Rejection: Reject if $N_{\sigma e-,TPC} < 3$
  - Pion Rejection: Reject if:
    - p < 0.65
      * if TOF and TPC available: $N_{\sigma \pi,TPC} < 3$ & $N_{\sigma \pi,TOF} < 3$
      * else
        · p < 0.5: $N_{\sigma \pi,TPC} < 3$
        · $0.5 <$ p < 0.65: $N_{\sigma \pi,TPC} < 2$
    - $0.65 <$ p < 1.5: $N_{\sigma \pi,TPC} < 5$ & $N_{\sigma \pi,TOF} < 3$
    - p > 1.5: $N_{\sigma \pi,TPC} < 5$ & $N_{\sigma \pi,TOF} < 2$

The purity of the $K^{\pm}$ collections was estimated using the MC data, for which the true identity of each reconstructed $K^{\pm}$ particle is known. Therefore, the purity may be estimated as:

$$Purity(K^{\pm}) = \frac{N_{true}}{N_{reconstructed}} \tag{1}$$

Purity(K^{+}) $\approx$ Purity(K^{-}) $\approx 97\%$

3.3 V0 Selection

Λ ($\bar{\Lambda}$) and K^0_S are neutral particles which cannot be directly detected, but must instead be reconstructed through detection of their decay products, or daughters. This process is illustrated in Figure 1. In general, particles which are topologically reconstructed in this fashion are called V0 particles. The class AliFemtoV0TrackCutNSigmaFilter (which is an extension of AliFemtoV0TrackCut) is used to reconstruct the V0s.

In order to obtain a true and reliable signal, one must ensure good purity of the V0 collection. The purity of the collection is calculated as:

$$Purity = \frac{Signal}{Signal + Background} \tag{2}$$

In order to obtain both the signal and background, the invariant mass distribution (M_{inv}) of all V0 candidates must be constructed immediately before the final invariant mass cut. Examples of such distribtions can be found in Figures 3 and 5. It is vital that this distribution be constructed immediately before the final M_{inv} cut, otherwise it would be impossible to estimate the background. As shown in Figures 3 and 5, the background is fit (with a polynomial) outside of the peak region of interest to obtain an estimate for the backfround within the region. Within the M_{inv} cut limits, the background is the region below the fit while the signal is the region above the fit.

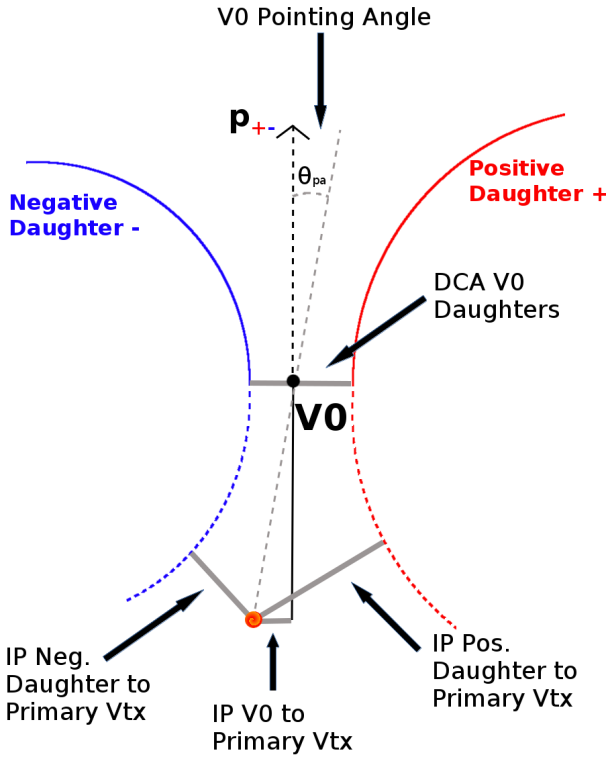

Fig. 1: V0 Reconstruction

3.3.1 Λ Reconstruction

The following cuts were used to select good Λ ($\bar{\Lambda}$) candidates:

1. Daughter Particle Cuts

(a) Cuts Common to Both Daughters

i. $|\eta| < 0.8$

ii. SetTPCnclsDaughters(80)

iii. SetStatusDaughters(AliESDtrack::kTPCrefic)

iv. SetMaxDcaV0Daughters(0.4)

(b) Pion Specific Daughter Cuts

i. $p_T > 0.16$

ii. DCA to prim vertex > 0.3

(c) Proton Specific Daughter Cuts

i. $p_T > 0.5(p)$ [$0.3(\bar{p})$] GeV/c

ii. DCA to prim vertex > 0.1

2. V0 Cuts

(a) $|\eta| < 0.8$

(b) $p_T > 0.4$

(c) $|m_{inv} - m_{PDG}| < 3.8$ MeV

(d) Cosine of pointing angle > 0.9993

(e) OnFlyStatus = false

(f) Decay Length < 60 cm

3. Shared Daughter Cut for V0 Collection

– Iterate through V0 collection to ensure that no daughter is used in more than one V0 candidate

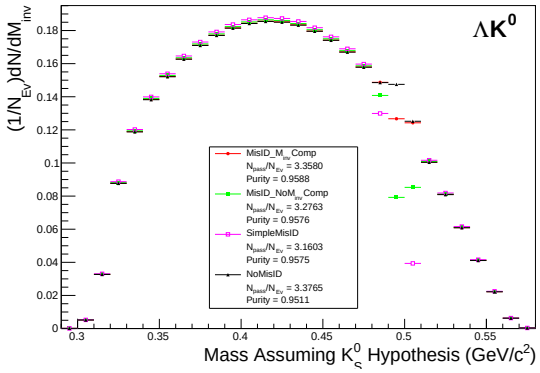

(a) Mass assuming K^0_S-hypothesis for Λ collection, i.e. assume the daughters are $\pi^+\pi^-$ instead of $p^+\pi^-$.

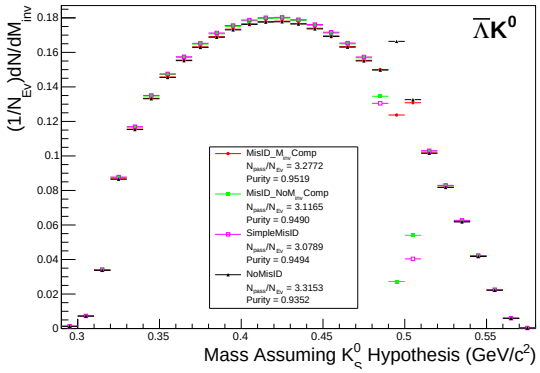

(b) Mass assuming K^0_S-hypothesis for $\bar{\Lambda}$ collection, i.e. assume the daughters are $\pi^+\pi^-$ instead of $\pi^+\bar{p}^-$.

Fig. 2: Mass assuming K^0_S-hypothesis for V0 candidates passing all Λ (2a) and $\bar{\Lambda}$ (2b) cuts. The "NoMisID" distribution (black triangles) uses the V0 finder without any attempt to remove misidentified K^0_S. The slight peak in the "NoMisID" distribution around $m_{inv} = 0.5$ GeV/c^2 contains misidentified K^0_S particles in our $\Lambda(\bar{\Lambda})$ collection. "SimpleMisID" (pink squares) simply cuts out the entire peak, which throws away some good Λ and $\bar{\Lambda}$ particles. "MisID_NoM$_{inv}$Comp" (green squares) uses the misidentification cut outlined in the text, but does not utilize the invariant mass comparison method. "MisID_M$_{inv}$Comp" (red circles) utilizes the full misidentification methods, and is currently used for this analysis. "N$_{pass}$/N$_{ev}$" is the total number of $\Lambda(\bar{\Lambda})$ particles found, normalized by the total number of events. The purity of the collection is also listed.

Figure 2a shows the mass assuming K^0_S hypothesis for the Λ collection, i.e. assume the daughters are $\pi^+\pi^-$ instead of $\pi^+\bar{p}^-$. Figure 2b is a similar plot, but is for the $\bar{\Lambda}$ collection, i.e. assume the daughters are $\pi^+\pi^-$ instead of $\pi^+\bar{p}^-$. The K^0_S contamination is visible, although not profound, in both in the slight peaks around m_{inv} = 0.497 GeV/c^2. If one simply cuts out the entire peak, good Λ particles will be lost. Ideally, the Λ selection and K^0_S misidentification cuts are selected such that the peak is removed from this plot while leaving the distribution continuous. To attempt to remove these K^0_S contaminations without throwing away good Λ and $\bar{\Lambda}$ particles, the following misidentification cuts are imposed; a Λ($\bar{\Lambda}$) candidate is rejected if all of the following criteria are satisfied:

- $\left|m_{inv,\ K^0_S\ Hypothesis} - m_{PDG,\ K^0_S}\right| < 9.0$ MeV/c^2
- Positive and negative daughters pass π daughter cut implemented for K^0_S reconstruction
- $\left|m_{inv,\ K^0_S\ Hypothesis} - m_{PDG,\ K^0_S}\right| < \left|m_{inv,\ \Lambda(\bar{\Lambda})\ Hypothesis} - m_{PDG,\ \Lambda(\bar{\Lambda})}\right|$

Figure 3 shows the invariant mass (M_{inv}) distribution of all Λ($\bar{\Lambda}$) candidates immediately before the final invariant mass cut. These distributions are used to calculate the collection purities. The Λ and $\bar{\Lambda}$ purities are found to be: Purity(Λ) ≈ Purity($\bar{\Lambda}$) ≈ 95%.

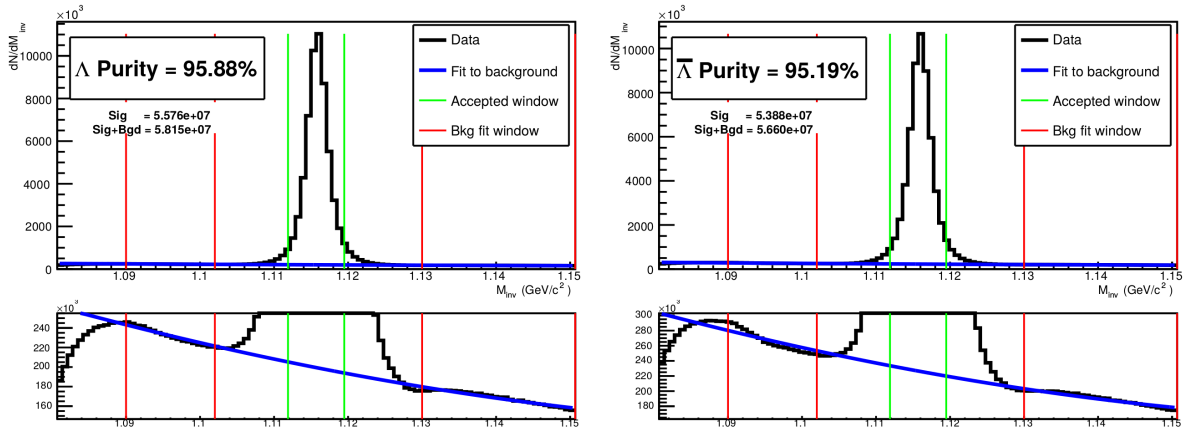

(a) Λ Purity (b) $\bar{\Lambda}$ Purity

Fig. 3: Invariant mass (M_{inv}) distribution of all Λ (a) and $\bar{\Lambda}$ (b) candidates immediately before the final invariant mass cut. The bottom figures are zoomed to show the background with fit. The vertical green lines represent the M_{inv} cuts used in the analyses, the red vertical lines delineate the region over which the background was fit, and the blue line shows the background fit. These distributions are used to calculate the collection purities, Purity(Λ) ≈ Purity($\bar{\Lambda}$) ≈ 95%.

3.3.2 K^0_S Reconstruction

The following cuts were used to select good K^0_S candidates:

1. Pion Daughter Cuts
   (a) $|\eta| < 0.8$
   (b) SetTPCnclsDaughters(80)
   (c) SetStatusDaughters(AliESDtrack::kTPCrefic)
   (d) SetMaxDcaV0Daughters(0.3)

(e) $p_T > 0.15$

(f) DCA to prim vertex > 0.3

2. K^0_S Cuts

(a) $|\eta| < 0.8$

(b) $p_T > 0.2$

(c) $m_{PDG} - 13.677$ MeV $< m_{inv} < m_{PDG} + 2.0323$ MeV

(d) Cosine of pointing angle > 0.9993

(e) OnFlyStatus = false

(f) Decay Length < 30 cm

3. Shared Daughter Cut for V0 Collection

– Iterate through V0 collection to ensure that no daughter is used in more than one V0 candidate

As can be seen in Figure 4, some misidentified Λ and $\bar{\Lambda}$ particles contaminate our K^0_S sample. Figure 4a shows the mass assuming Λ-hypothesis for the K^0_S collection, i.e. assume the daughters are $p^+\pi^-$ instead of $\pi^+\pi^-$. Figure 4b is similar, but shows the mass assuming $\bar{\Lambda}$ hypothesis for the collection, i.e. assume the daughters are $\pi^+\bar{p}^-$ instead of $\pi^+\pi^-$. The Λ contamination can be seen in 4a, and the $\bar{\Lambda}$ contamination in 4b, in the peaks around $m_{inv} = 1.115$ GeV/c^2. Additionally, the $\bar{\Lambda}$ contamination is visible in Figure 4a, and the Λ contamination visible in Figure 4b, in the region of excess around $1.65 < m_{inv} < 2.1$ GeV/c^2. This is confirmed as the number of misidentified Λ particles in the sharp peak of Figure 4a (misidentified $\bar{\Lambda}$ particles in the sharp peak of Figure 4b) approximately equals the excess found in the $1.65 < m_{inv} < 2.1$ GeV/c^2 region of Figure 4a (Figure 4b).

The peaks around $m_{inv} = 1.115$ GeV/c^2 in Figure 4 contain both misidentified Λ ($\bar{\Lambda}$) particles and good K^0_S. If one simply cuts out the entire peak, some good K^0_S particles will be lost. Ideally, the K^0_S selection and $\Lambda(\bar{\Lambda})$ misidentification cuts can be selected such that the peak is removed from this plot while leaving the distribution continuous. To attempt to remove these Λ and $\bar{\Lambda}$ contaminations without throwing away good K^0_S particles, the following misidentification cuts are imposed; a K^0_S candidate is rejected if all of the following criteria are satisfied (for either Λ or $\bar{\Lambda}$ hypothesis):

– $\left| m_{inv,\ \Lambda(\bar{\Lambda})\ Hypothesis} - m_{PDG,\ \Lambda(\bar{\Lambda})} \right| < 9.0$ MeV/c^2

– Positive daughter passes $p^+(\pi^+)$ daughter cut implemented for $\Lambda(\bar{\Lambda})$ reconstruction

– Negative daughter passes $\pi^-(\bar{p}^-)$ daughter cut implemented by $\Lambda(\bar{\Lambda})$ reconstruction

– $\left| m_{inv,\ \Lambda(\bar{\Lambda})\ Hypothesis} - m_{PDG,\ \Lambda(\bar{\Lambda})} \right| < \left| m_{inv,\ K^0_S\ Hypothesis} - m_{PDG,\ K^0_S} \right|$

3.4 Cascade Reconstruction

The reconstruction of Ξ particles is one step above V0 reconstruction. V0 particles are topologically reconstructed by searching for the charged daughters' tracks into which they decay. With Ξ particles, we search for the V0 particle and charged daughter into which the Ξ decays. In the case of Ξ^-, we search for the Λ (V0) and π^- (track) daughters. We will refer to this π as the "bachelor π". The reconstruction of Ξ, and the specific cuts used will be included in future versions of this note.

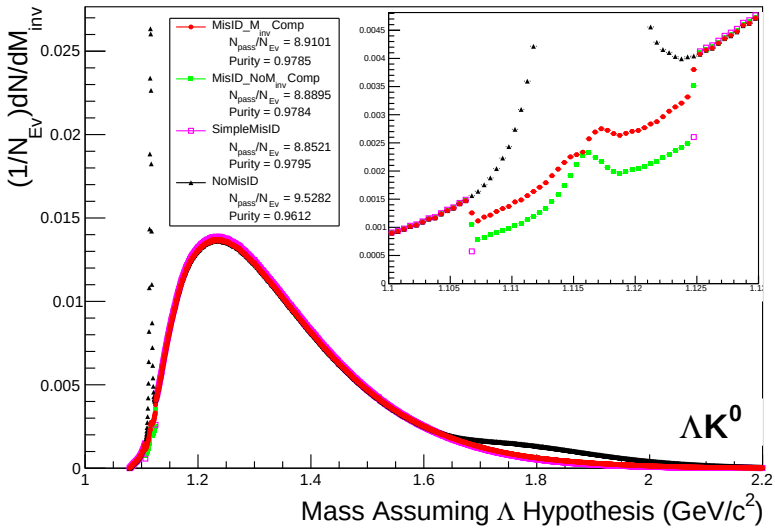

(a) Mass assuming Λ-hypothesis for K^0_S collection, i.e. assume the daughters are $p^+\pi^-$ instead of $\pi^+\pi^-$.

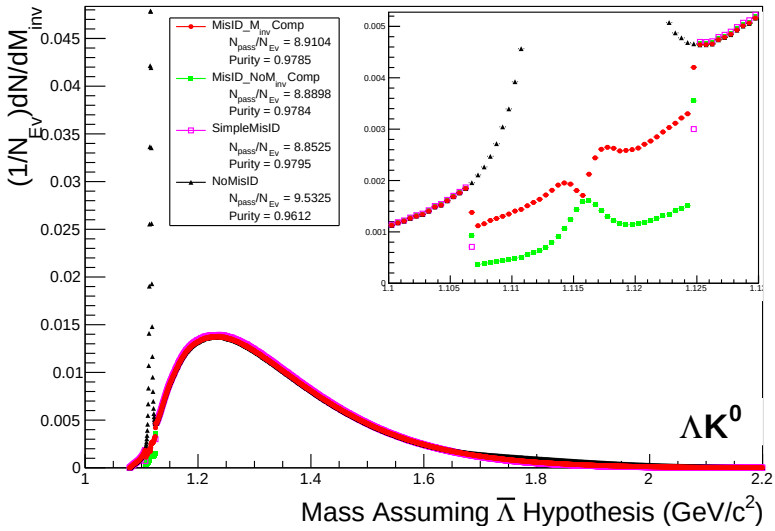

(b) Mass assuming $\bar{\Lambda}$-hypothesis for K^0_S collection, i.e. assume the daughters are $\pi^+\bar{p}^-$ instead of $\pi^+\pi^-$.

Fig. 4: Mass assuming Λ-hypothesis (4a) and $\bar{\Lambda}$-hypothesis (4b) for K^0_S collection. The "NoMisID" distribution (black triangles) uses the V0 finder without any attempt to remove misidentified Λ and $\bar{\Lambda}$. The peak in the "NoMisID" distribution around $m_{inv} = 1.115$ GeV/c^2 contains misidentified Λ (4a) and $\bar{\Lambda}$ (4b) particles in our K^0_S collection. "SimpleMisID" (pink squares) simply cuts out the entire peak, which throws away some good K^0_S particles. "MisID_NoM$_{inv}$Comp" (green squares) uses the misidentification cut outlined in the text, but does not utilize the invariant mass comparison method. "MisID_M$_{inv}$Comp" (red circles) utilizes the full misidentification methods, and is currently used for this analysis. "N$_{pass}$/N$_{ev}$" is the total number of K^0_S particles found, normalized by the total number of events. The purity of the collection is also listed. Also note, the relative excess of the "NoMisID" distribution around $1.65 < m_{inv} < 2.1$ GeV/c^2 shows misidified $\bar{\Lambda}$ (4a) and Λ (4b) particles in our K^0_S collection.

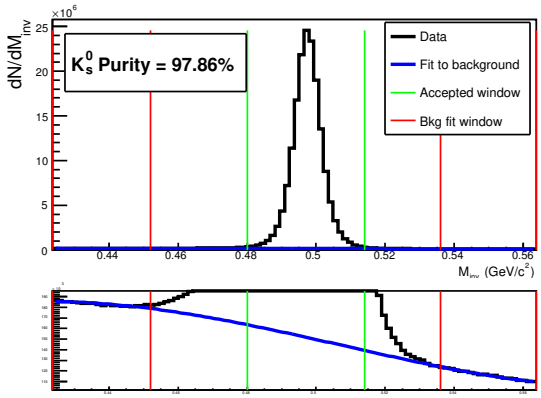

Fig. 5: Invariant mass (M_{inv}) distribution of all K^0_S candidates immediately before the final invariant mass cut. The bottom figure is zoomed to show the background with fit. The vertical green lines represent the M_{inv} cut used in the analyses, the red vertical lines delineate the region over which the background was fit, and the blue line shows the background fit. This distribution is used to calculate the collection purity, Purity(K^0_S) $\approx 98\%$.

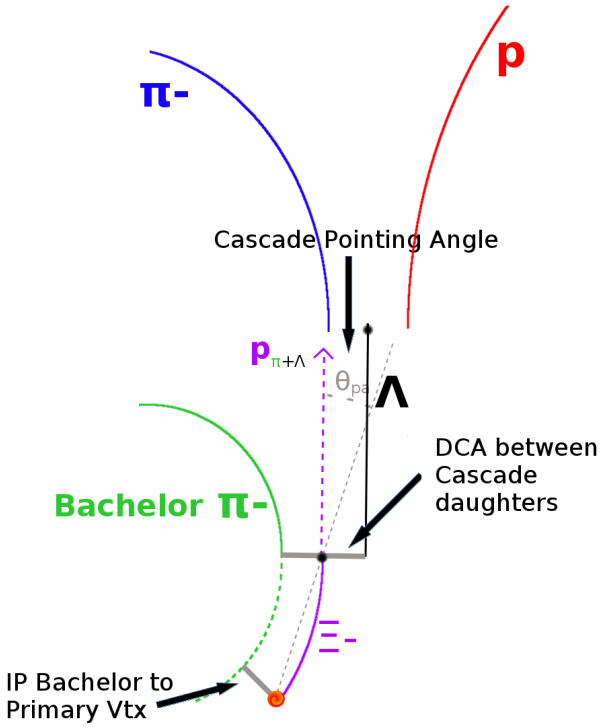

Fig. 6: Ξ Reconstruction

3.5 Pair Selection

It is important to obtain true particle pairs in the analysis. In particular, contamination from pairs constructed with split or merged tracks, and pairs sharing daughters, can introduce an artificial signal into the correlation function, obscuring the actual physics.

1. Shared Daughter Cut for Pairs
   (a) V0-V0 Pairs (i.e. $\Lambda(\bar{\Lambda})K^0_S$ analyses)
      – Remove all pairs which share a daughter
      – Ex. Λ and K^0_S particles which share a π^- daughter are not included

(b) V0-Track Pairs (i.e. $\Lambda(\bar{\Lambda})\mathrm{K}^{\pm}$ analyses

- Remove pairs if Track is also used as a daughter of the V0
- In these analyses, this could only occur if, for instance, a K is misidentified as a π or p in the V0 reconstruction

2. Average Separation Cuts

- Used to cut out splitting and merging effects
- The motivation for these cuts can be seen in Figures 7 and 8, in which average separation correlation functions are presented

(a) $\Lambda(\bar{\Lambda})\mathrm{K}^0_S$ Analyses

- Average separation > 6.0 cm for like charge sign daughters
  - ex. p daughter of Λ and π^+ daughter of K^0_S
- No cut for unlike-sign daughters

(b) $\Lambda(\bar{\Lambda})\mathrm{K}^{\pm}$ Analyses

- Average Separation > 8.0 cm for daughter of $\Lambda(\bar{\Lambda})$ sharing charge sign of $\mathrm{K}^{\pm}$
  - ex. in $\Lambda\mathrm{K}^+$ analysis, p daughter of Λ with K^+
- No cut for unlike signs

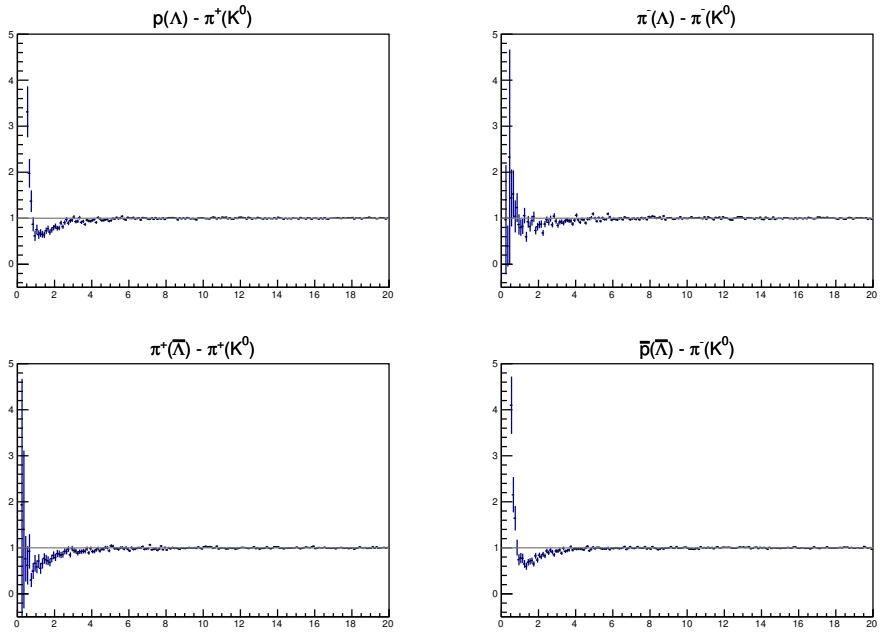

Fig. 7: Avgerage separation (cm) correlation functions of $\Lambda(\bar{\Lambda})$ and K^0_S Daughters. Only like-sign daughter pairs are shown (the distributions for unlike-signs were found to be flat). The title of each subfigure shows the daughter pair, as well as the mother of each daughter (in "()"), ex. top left is p from Λ with π^+ from K^0_S.

4 Correlation Functions

This analysis studies the momentum correlations of both Λ-K and Ξ-K pairs using the two-particle correlation function, defined as $C(k^*) = A(k^*)/B(k^*)$, where $A(k^*)$ is the signal distribution, $B(k^*)$ is the reference (or background) distribution, and k^* is the momentum of one of the particles in the pair rest

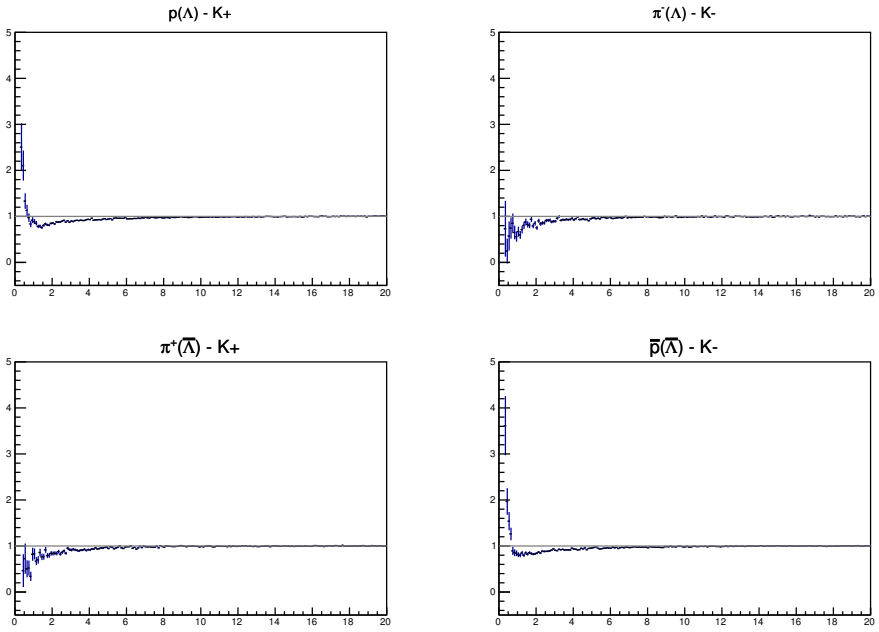

Fig. 8: Avgerage separation (cm) correlation functions of $\Lambda(\bar{\Lambda})$ Daughter and $K^{\pm}$. Only like-sign pairs are shown (unlike-signs were flat). In the subfigure titles, the particles in "()" represent the mothers, ex. top left is p from Λ with K^{+}.

frame. In practice, $A(k^*)$ is constructed by binning in k^* pairs from the same event. Ideally, $B(k^*)$ is similar to $A(k^*)$ in all respects excluding the presence of femtoscopic correlations [2]; as such, $B(k^*)$ is used to divide out the phase-space effects, leaving only the femtoscopic effects in the correlation function.

In practice, $B(k^*)$ is obtained by forming mixed-event pairs, i.e. particles from a given event are paired with particles from $N_{mix}(= 5)$ other events, and these pairs are then binned in k^*. In forming the background distribution, it is important to mix only similar events; mixing events with different phase-spaces can lead to artificial signals in the correlaton function. Therefore, in this analysis, we mix events with primary vertices within 2 cm and centralities within 5% of each other. Also note, a vertex correction is also applied to each event, which essentially recenters the the primary vertices to z = 0.

This analysis presents correlation functions for three centrality bins (0-10%, 10-30%, and 30-50%), and is currently pair transverse momentum ($k_T = 0.5|\mathbf{p}_{T,1} + \mathbf{p}_{T,2}|$) integrated (i.e. not binned in k_T). The correlation functions are constructed separately for the two magnetic field configurations, and are combined using a weighted average:

$$C_{combined}(k^*) = \frac{\sum_i w_i C_i(k^*)}{\sum_i w_i} \tag{3}$$

where the sum runs over the correlation functions to be combined, and the weight, w_i, is the number of numerator pairs in $C_i(k^*)$. Here, the sum is over the two field configurations.

Figures 9, 10, and 11 show the correlation functions for all centalities studied for $\Lambda K^0_S(\bar{\Lambda}K^0_S)$, $\Lambda K^+(\bar{\Lambda}K^-)$, and $\Lambda K^-(\bar{\Lambda}K^+)$, respectively.

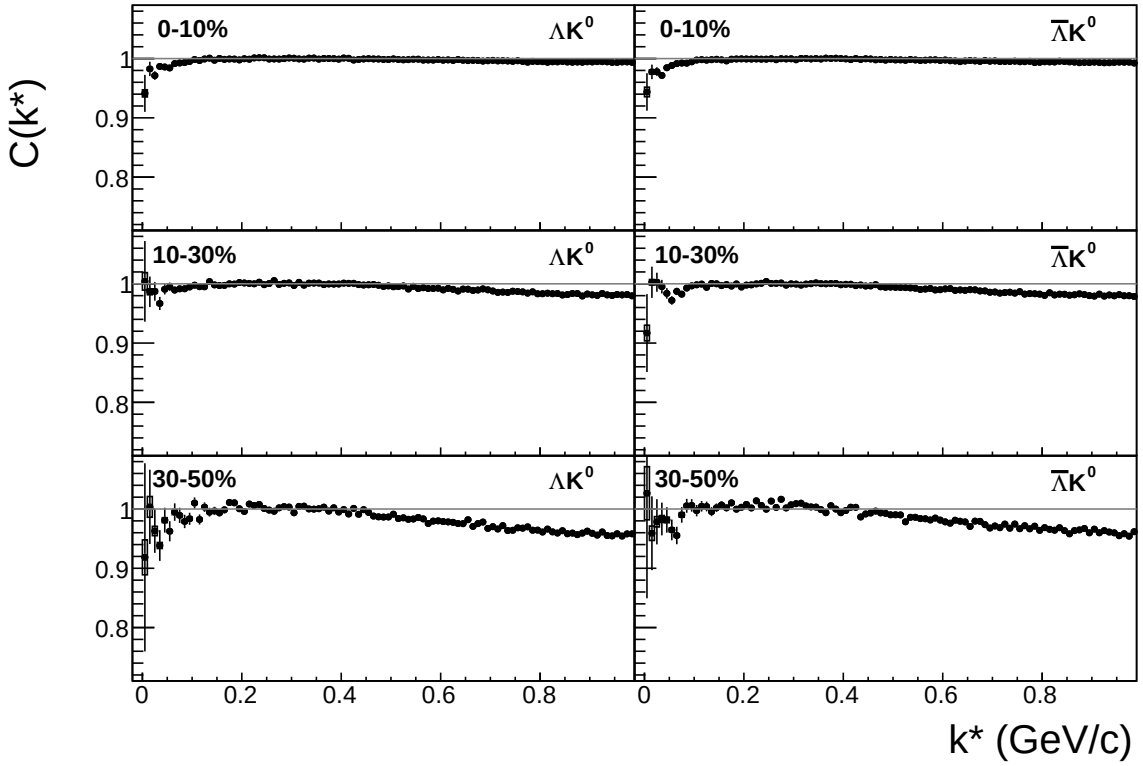

Fig. 9: ΛK^0_S (left) and $\bar{\Lambda} K^0_S$ (right) correlation functions for 0-10% (top), 10-30%(middle), and 30-50%(bottom) centralities.

5 Fitting

5.1 Model: ΛK^0_S, $\Lambda K^{\pm}$, $\Xi^{ch} K^0_S$

In the absence of Coulomb effects, and assuming a spherically gaussian source of width R, the 1D femtoscopic correlation function can be calculated analytically using:

$$C(k^*) = 1 + \lambda [C_{QI}(k^*) + C_{FSI}(k^*)] \tag{4}$$

C_{QI} describes plane-wave quantum interference:

$$C_{QI}(k^*) = \alpha \exp(-4k^{*2}R^2) \tag{5}$$

where $\alpha = (-1)^{2j}/(2j+1)$ for identical particles with spin j, and $\alpha = 0$ for non-identical particles. Obviously, $\alpha = 0$ for all analyses presented in this note. C_{FSI} describes the s-wave strong final state interaction between the particles:

$$\begin{gathered} C_{FSI}(k^*) = (1+\alpha)[\tfrac{1}{2}|\tfrac{f(k^*)}{R}|^2(1-\tfrac{d_0}{2\sqrt{\pi}R}) + \tfrac{2\mathbb{R}f(k^*)}{\sqrt{\pi}R}F_1(2k^*R) - \tfrac{\mathbb{I}f(k^*)}{R}F_2(2k^*R)] \\ f(k^*) = (\tfrac{1}{f_0} + \tfrac{1}{2}d_0k^{*2} - ik^*)^{-1}; \quad F_1(z) = \int_0^z \tfrac{e^{x^2-z^2}}{z}dx; \quad F_2(z) = \tfrac{1-e^{-z^2}}{z} \end{gathered} \tag{6}$$

where R is the source size, $f(k^*)$ is the s-wave scattering amplitude, f_0 is the complex scattering length, and d_0 is the effective range of the interaction.

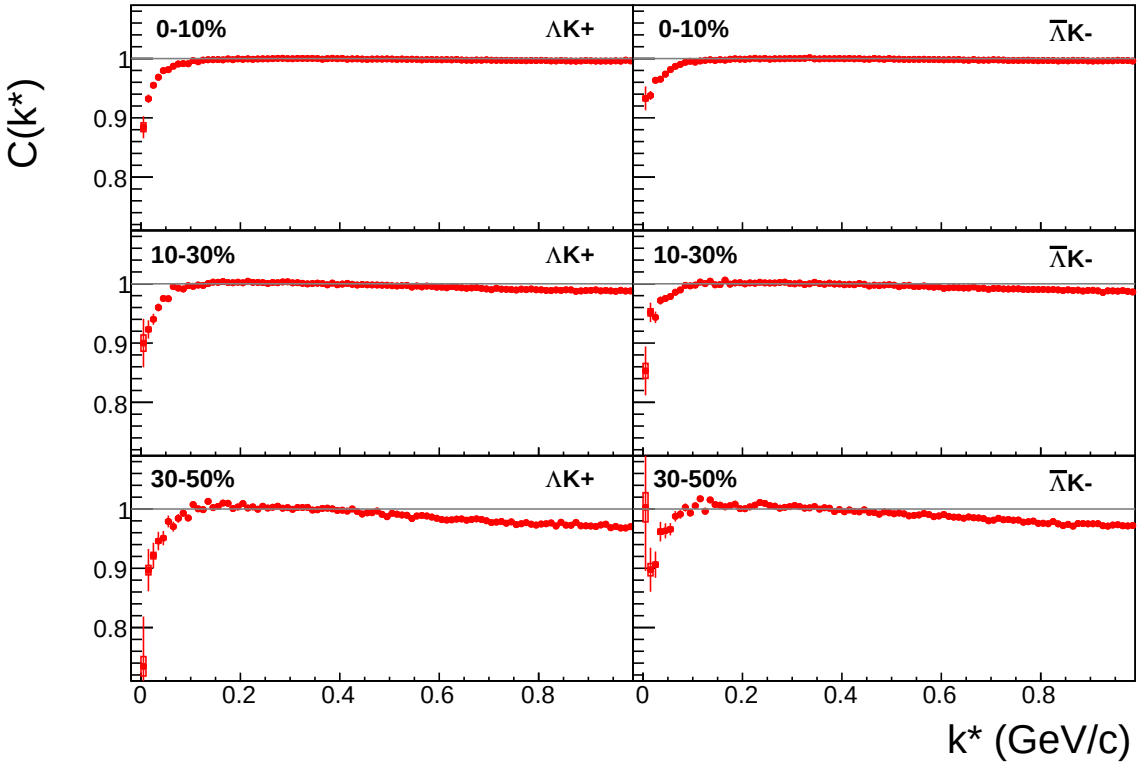

Fig. 10: ΛK^+ (left) and $\bar{\Lambda}K^-$ (right) correlation functions for 0-10% (top), 10-30%(middle), and 30-50%(bottom) centralities.

The code developed to fit the data is called "LednickyFitter", and utilizes the ROOT TMinuit implementation of the MINUIT fitting package. In short, given a function with a number of parameters, the fitter explores the parameter space searching for the minimum of the equation. In this implementation, the function to be minimized should represent the difference between the measure and theoretical correlation functions. However, a simple χ^2 test in inappropriate for fitting correlation functions, as the ratio two Poisson distributions does not result in a Poisson distribution. Instead, a log-likelihood fit function of the following form is used [2]:

$$\chi^2_{PML} = -2\left[A\ln\left(\frac{C(A+B)}{A(C+1)}\right) + B\ln\left(\frac{A+B}{B(C+1)}\right)\right] \tag{7}$$

where A is the experimental signal distribution (numerator), B is the experimental background distribution (denominator), and C is the theoretical fit correlation function.

The LednickyFitter uses Equations 4 – 6 to build the theoretical fit, and Equation 7 as the statistic quantifying the quality of the fit. The parameters to be varied by MINUIT are: λ, R, f_0 ($\mathbb{R}f_0$ and $\mathbb{I}f_0$ separately), d_0, and normalization N. The fitter currently includes methods to correct for momentum resolution and a non-flat background. These corrections are applied to the fit function, the data is never touched. The fitter is able to share parameters between different analyses and fit all simultaneously.

In a typical fit, a given pair is fit with its conjugate (ex. ΛK^+ with $\bar{\Lambda}K^-$) across all centralities (0-10%, 10-30%, 30-50%), for a total of 6 simultaneous analyses. Each analysis has a unique λ and normalization parameter. The radii are shared between analyses of like centrality, as these should have similar source sizes. The scattering parameters ($\mathbb{R}f_0$, $\mathbb{I}f_0$, d_0) are shared amongst all.

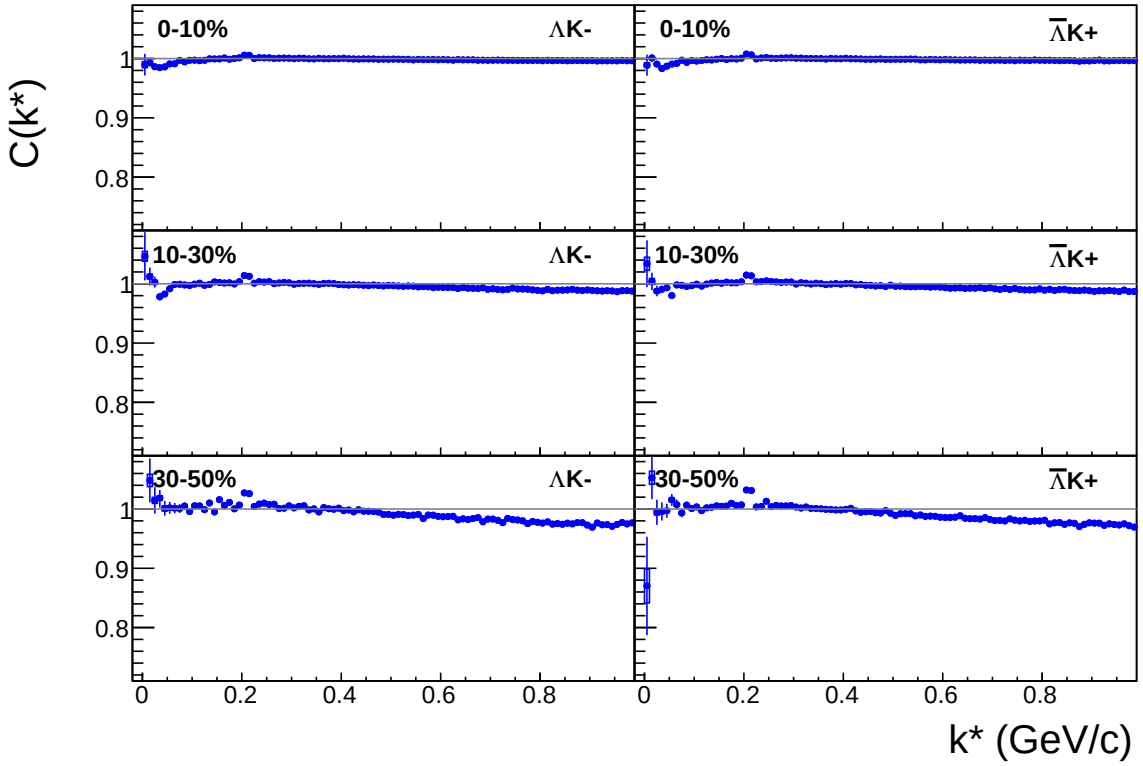

Fig. 11: ΛK^- (left) and $\bar{\Lambda}K^+$ (right) correlation functions for 0-10% (top), 10-30%(middle), and 30-50%(bottom) centralities. The peak at k* $\approx$ 0.2 GeV/c is due to the Ω^- resonance.

Figures 13, 14, and 15 show experimental data with fits for all studied centralities for ΛK^0_S with $\bar{\Lambda}K^0_S$, ΛK^+ with $\bar{\Lambda}K^-$, and ΛK^- with $\bar{\Lambda}K^+$, respectively. In the figures, the black solid line represents the "raw" fit, i.e. not corrected for momentum resolution effects nor non-flat background. The green line shows the fit to the non-flat background. The purple points show the fit after momentum resolution and non-flat background corrections have been applied. The initial values of the parameters is listed, as well as the final fit values with uncertainties.

5.2 Model: $\Xi^{ch}K^{ch}$

When fitting the $\Xi^-(\bar{\Xi}^+)K^\pm$ results, it is necessary to include both strong and Coulomb effects. In this case, Equation 4 is no longer valid, and, in fact, there is no analytical form with which to fit. Therefore, we must begin with the wave function describing the pair interaction, and simulate many particle pairs to obtain a theoretical fit correlation function. The code developed to achieve this functionality is called "CoulombFitter". Currently, in order to generate the statistics needed for a stable fit, we find that $\sim 10^4$ simulated pairs per 10 MeV bin are necessary. Unfortunately, the nature of this process means that the "CoulombFitter" takes much longer to run than the "LednickyFitter" of Section 5.1.

The two-particle correlation function may be written as:

$$C(\mathbf{k}^*) = \sum_S \rho_S \int S(\mathbf{r}^*)|\Psi^S_{\mathbf{k}^*}(\mathbf{r}^*)|^2 d^3\mathbf{r}^* \tag{8}$$

where ρ_S is the normalized emission probability of particles in a state with spin S, $S(\mathbf{r}^*)$ is the pair emission source distribution (assumed to be Gaussian), and $\Psi^S_{\mathbf{k}^*}(\mathbf{r}^*)$ is the two-particle wave-function including both strong and Coulomb interactions [3]:

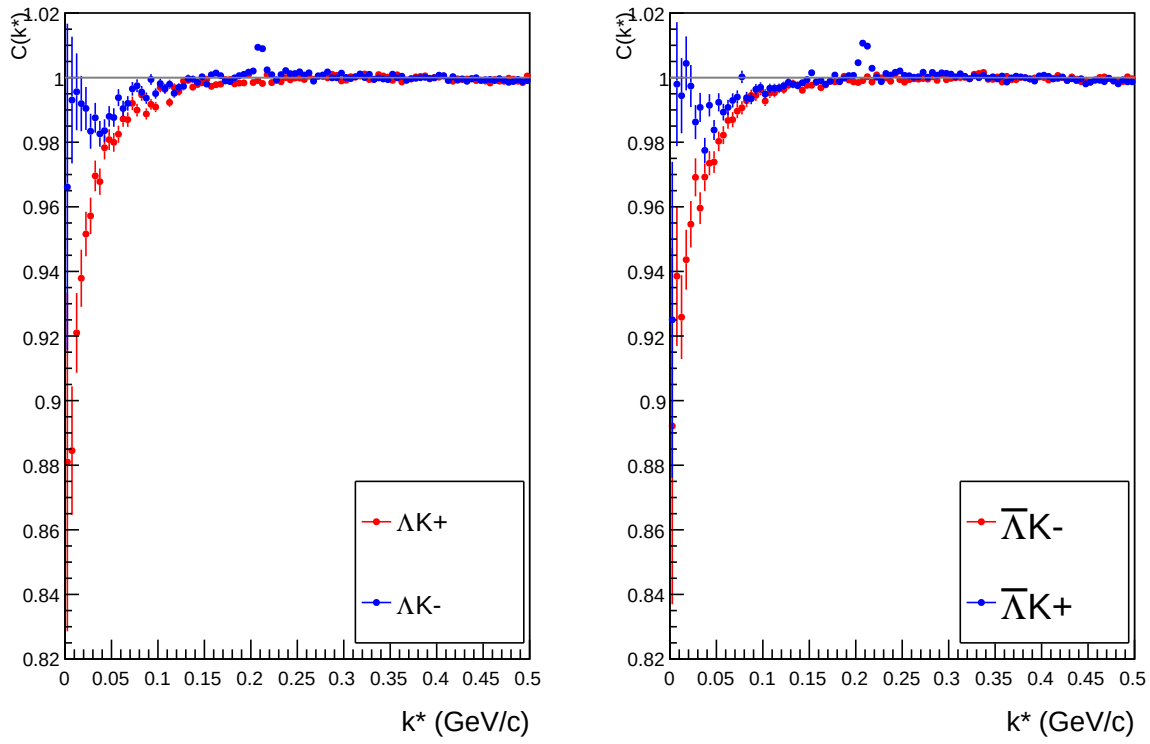

Fig. 12: Correlation Functions: ΛK^+ vs ΛK^- ($\bar{\Lambda}K^+$ vs $\bar{\Lambda}K^-$) for 0-10% centrality. The peak in ΛK^-($\bar{\Lambda}K^+$) at k* $\approx$ 0.2 GeV/c is due to the Ω^- resonance.

$$\Psi_{\mathbf{k}^*}(\mathbf{r}^*) = e^{i\delta_c}\sqrt{A_c(\eta)}[e^{i\mathbf{k}^*\cdot\mathbf{r}^*}F(-i\eta,1,i\xi) + f_c(k^*)\frac{\tilde{G}(\rho,\eta)}{r^*}] \tag{9}$$

where $\rho = k^* r^*$, $\eta = (k^* a_c)^{-1}$, $\xi = \mathbf{k}^*\cdot\mathbf{r}^* + k^* r^* \equiv \rho(1+\cos\theta^*)$, and $a_c = (\mu z_1 z_2 e^2)^{-1}$ is the two-particle Bohr radius (including the sign of the interaction). δ_c is the Coulomb s-wave phase shift, $A_c(\eta)$ is the Coulomb penetration factor, $\tilde{G} = \sqrt{A_c}(G_0 + iF_0)$ is a combination of the regular (F_0) and singular (G_0) s-wave Coulomb functions. $f_c(k^*)$ is the s-wave scattering amplitude:

$$f_c(k^*) = [\frac{1}{f_0} + \frac{1}{2}d_0 k^{*2} - \frac{2}{a_c}h(\eta) - ik^* A_c(\eta)]^{-1} \tag{10}$$

where, the "h-function", $h(\eta)$, is expressed through the digamma function, $\psi(z) = \Gamma'(z)/\Gamma(z)$ as:

$$h(\eta) = 0.5[\psi(i\eta) + \psi(-i\eta) - \ln(\eta^2)] \tag{11}$$

As stated before, to generate a fit correlation function, we must simulate a large number of pairs, calculate the wave-function, and average Ψ^2 over all pairs in a given k* bin. Essentially, we calculate Equation 8 by hand:

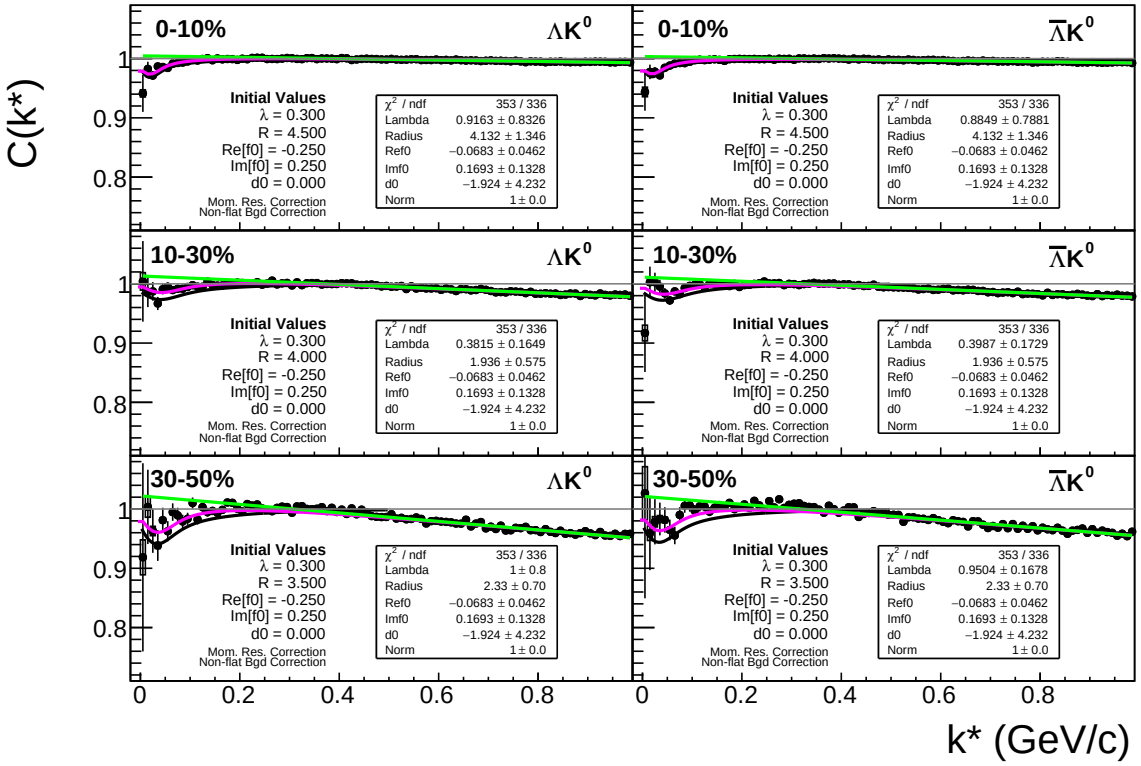

Fig. 13: Fits to the ΛK^0_S (left) and $\bar{\Lambda}K^0_S$ (right) data for the centralities 0-10% (top), 10-30% (middle), and 30-50% (bottom). Each has unique λ and normalization parameters. The radii are shared amongst like centralities; the scattering parameters ($\mathbb{R}f_0$, $\mathbb{I}f_0$, d_0) are shared amongst all. The black solid line represents the "raw" fit, i.e. not corrected for momentum resolution effects nor non-flat background. The green line shows the fit to the non-flat background. The purple points show the fit after momentum resolution and non-flat background corrections have been applied. The initial values of the parameters is listed, as well as the final fit values with uncertainties.

$$
\begin{aligned}
C(\mathbf{k}^*) &= \sum_S \rho_S \int S(\mathbf{r}^*) |\Psi^S_{\mathbf{k}^*}(\mathbf{r}^*)|^2 d^3\mathbf{r}^* \\
&\longrightarrow C(|\mathbf{k}^*|) \equiv C(k^*) = \sum_S \rho_S \langle |\Psi^S(\mathbf{k}^*_\mathbf{i}, \mathbf{r}^*_\mathbf{i})|^2 \rangle_i \\
&\longrightarrow C(k^*) = \lambda \sum_S \rho_S \langle |\Psi^S(\mathbf{k}^*_\mathbf{i}, \mathbf{r}^*_\mathbf{i})|^2 \rangle_i + (1-\lambda)
\end{aligned}
\tag{12}
$$

where $\langle\rangle_i$ represents an average over all pairs in a given k* bin.

In summary, for a given k* bin, we must draw $N_{pairs} \sim 10^4$ pairs, and for each pair:

1. Draw a random $\mathbf{r}^*$ vector according to our Gaussian source distribution $S(\mathbf{r}^*)$
2. Draw a random $\mathbf{k}^*$ vector satisfying the $|\mathbf{k}^*|$ restriction of the bin
   - We draw from real k^* vectors obtained from the data
   - However, we find that drawing from a distribution flat in k^* gives similar results
3. Construct the wave-function Ψ

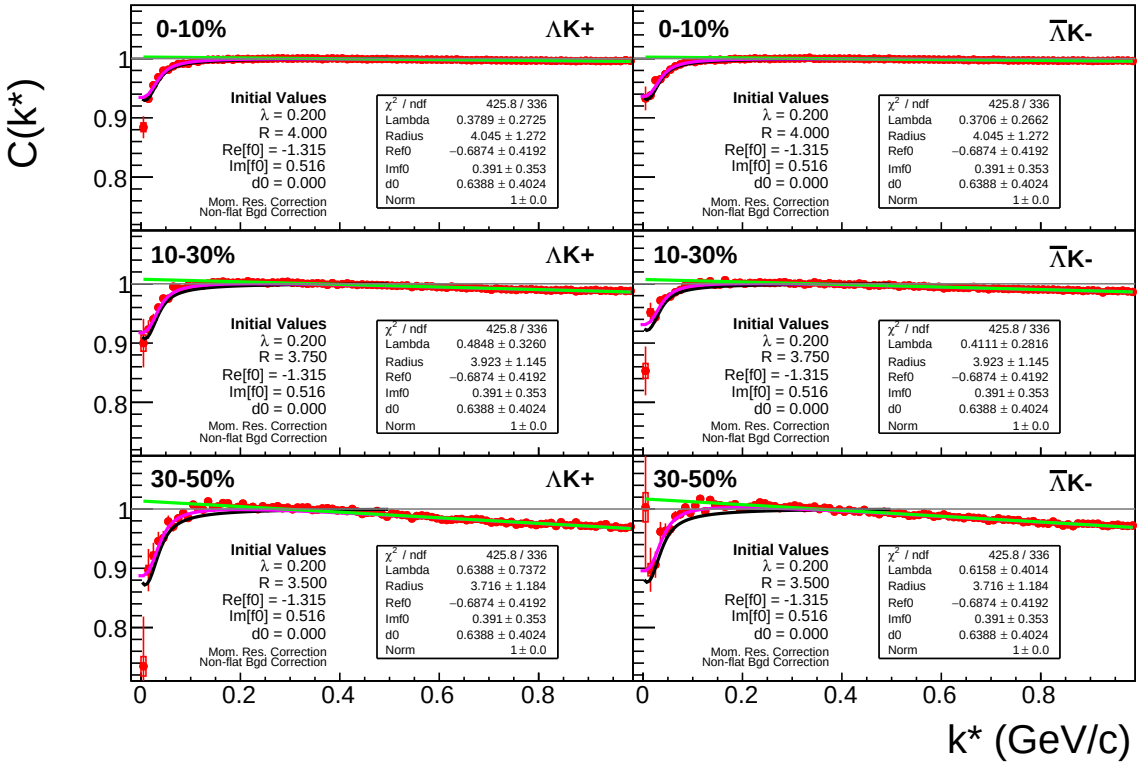

Fig. 14: Fits to the ΛK^+ (left) and $\bar{\Lambda} K^-$ (right) data for the centralities 0-10% (top), 10-30% (middle), and 30-50% (bottom). Each has unique λ and normalization parameters. The radii are shared amongst like centralities; the scattering parameters ($\mathbb{R}f_0$, $\mathbb{I}f_0$, d_0) are shared amongst all. The black solid line represents the "raw" fit, i.e. not corrected for momentum resolution effects nor non-flat background. The green line shows the fit to the non-flat background. The purple points show the fit after momentum resolution and non-flat background corrections have been applied. The initial values of the parameters is listed, as well as the final fit values with uncertainties.

After all pairs for a given k* bin are simulated and wave-functions obtained, the results are averaged to give the fit result.

Construction of the wave-functions, Equation 9, involves a number of complex functions not included in standard C++ or ROOT libraries (namely, $h(\eta)$, $\tilde{G}(\rho,\eta)$), and $F(-i\eta,1,i\xi)$. These functions were even difficult to find and implement from elsewhere. Our solution was to embed a Mathematica kernel into our C++ code to evaluate these functions. However, having Mathematica work on-the-fly with the fitter was far too time consuming (fitter would have taken day, maybe weeks to finish). Our solution was to use Mathematica to create matrices representing these functions for different parameter values. During fitting, these matrices were then interpolated and the results used to build the wave-functions. This method decreased the running time dramatically, and we are not able to generate results in under $\sim$ 1 hour. This process will be explained in more detail in future versions of the note.

5.3 Momentum Resolution Corrections

Finite track momentum resolution causes the reconstructed momentum of a particle to smear around the true value. This, of course, also holds true for V0 particles. The effect is propagated up to the pairs of interest, which causes the reconstructed relative momentum (k^*_{Rec}) to differ from the true momentum (k^*_{True}). Smearing of the momentum typically will result in a suppression of the signal.

The effect of finite momentum resolution can be investigated using the MC data, for which both the true

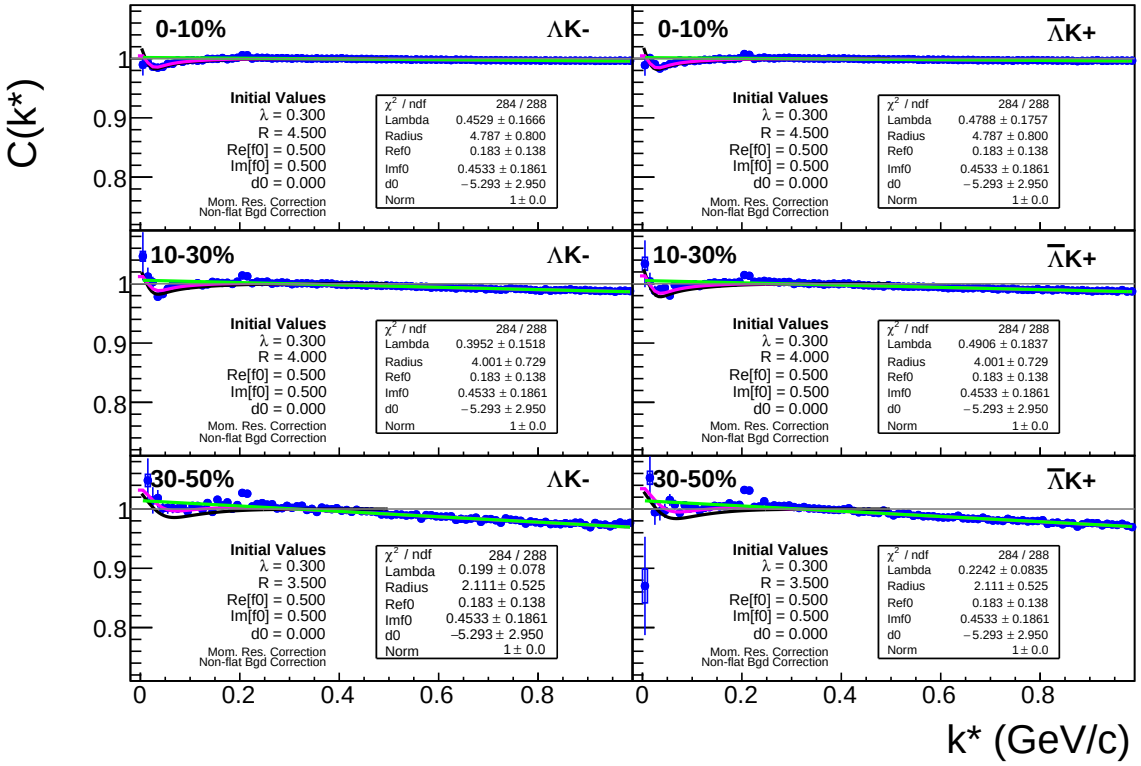

Fig. 15: Fits to the ΛK^-(left) with $\bar{\Lambda}K^+$ (right) data for the centralities 0-10% (top), 10-30% (middle), and 30-50% (bottom). Each has unique λ and normalization parameters. The radii are shared amongst like centralities; the scattering parameters ($\mathbb{R}f_0$, $\mathbb{I}f_0$, d_0) are shared amongst all. The black solid line represents the "raw" fit, i.e. not corrected for momentum resolution effects nor non-flat background. The green line shows the fit to the non-flat background. The purple points show the fit after momentum resolution and non-flat background corrections have been applied. The initial values of the parameters is listed, as well as the final fit values with uncertainties.

and reconstructed momenta are available. Figure 16 shows sample k^*_{True} vs. k^*_{Rec} plots for $\Lambda(\bar{\Lambda})K^{\pm}$ 0-10% analyses; Figure 16a was generated using same-event pairs, while Figure 16b was generated using mixed-event pairs (with $N_{mix} = 5$).

If there are no contaminations in our particle collection, the plots in Figure 16 should be smeared around $k^*_{True} = k^*_{Rec}$; this is mostly true in our analyses. However, there are some interesting features of our results which demonstrate a small (notice the log-scale on the z-axis) contamination in our particle collection. The structure around $k^*_{Rec} = k^*_{True} - 0.15$ is mainly caused by K^0_S contamination in our $\Lambda(\bar{\Lambda})$ sample. The remaining structure not distributed about $k^*_{Rec} = k^*_{True}$ is due to π and e contamination in our $K^{\pm}$ sample. These contaminations are more visible in Figure 17, which show k^*_{Rec} vs. k^*_{True} plots (for a small sample of the ΛK^+ 0-10% central analysis), for which the MC truth (i.e. true, known identity of the particle) was used to eliminate misidentified particles in the K^+(a) and Λ(b) collections. (NOTE: This is an old figure and is for a small sample of the data. A new version will be generated shortly. It, nonetheless, demonstrates the point well).

Information gained from looking at k^*_{Rec} vs k^*_{True} can be used to apply corrections to account for the effects of finite momentum resolution on the correlation functions. A typical method involves using the MC HIJING data to build two correlation functions, $C_{Rec}(k^*)$ and $C_{True}(k^*)$, using the generator-level momentum (k^*_{True}) and the measured detector-level momentum (k^*_{Rec}). The data is then corrected by multiplying by the ratio, C_{True}/C_{Rec}, before fitting. This essentially unsmears the data, which that can be compared directly to theoretical predictions and fits. Although this is conceptually simple, there are

a couple of big disadvantages to this method. First, HIJING does not incorporate final-state interactions, so weights must be used when building same-event (numerator) distributions. These weights account for the interactions, and, in the absence of Coulomb interactions, can be calculated using Eq. 4. Of course, these weights are valid only for a particular set of fit parameters. Therefore, in the fitting process, during which the fitter explores a large parameter set, the corrections will not remain valid. As such, applying the momentum resolution correction and fitting becomes a long and drawn out iterative process. An ititial parameter set is obtained (through fitting without momentum resolution corrections, theoretical models, or a good guess), then the MC data is run over to obtain the correction factor, the data is fit using the correction factor, a refined parameter set is extracted, the MC data is run over again to obtain the new correction factor, etc. This process continues until the parameter set stabilizes. The second issue concerns statistics. With the MC data available on the grid, we were not able to generate the statistics necessary to use the raw C_{True}/C_{Rec} ratio. The ratio was not stable, and when applied to the data, obscured the signal. Attempting to fit the ratioto use to generate the corrections also proved problematic. However, as HIJING does not include final-state interactions, the same-event and mixed-event pairs are very similiar (with the exception of things like energy and momentum conservation, etc). Therefore, one may build the numerator distribution using mixed-event pairs. This corresponds, more or less, to simply running a the weight generator through the detector framework.

A second approach is to use information gained from plots like those in Figure 16, which can be considered response matrices. The reponse matrix describes quantitatively how each k^*_{Rec} bin receives contributions from multiple k^*_{True} bins, and can be used to account for the effects of finite momentum resolution. With this approach, the resolution correction is applied on-the-fly during the fitting process by propagating the theoretical (fit) correlation function through the response matrix, according to:

$$C_{fit}(k^*_{Rec}) = \frac{\sum\limits_{k^*_{True}} M_{k^*_{Rec},k^*_{True}} C_{fit}(k^*_{True})}{\sum\limits_{k^*_{True}} M_{k^*_{Rec},k^*_{True}}} \tag{13}$$

where $M_{k^*_{Rec},k^*_{True}}$ is the response matrix (Figure 16), $C_{fit}(k^*_{True})$ is the fit binned in k^*_{True}, and the denominator normalizes the result.

Equation 13 describes that, for a given k^*_{Rec} bin, the observed value of $C(k^*_{Rec})$ is a weighted average of all $C(k^*_{True})$ values, where the weights are the normalized number of counts in the [k^*_{Rec}, k^*_{True}] bin. As seen in Figure 16, overwhelmingly the main contributions comes from the $k^*_{Rec} = k^*_{True}$ bins. Although the correction is small, it is non-negligible for the low-k* region of the correlation function.

Here, the momentum resolution correction is applied to the fit, not the data. In other words, during fitting, the theoretical correlation function is smeared just as real data would be, instead of unsmearing the data. This may not be ideal for the theorist attempting to compare a model to experimental data, but it leaves the experimental data unadulterated. The current analyses use this second approach to applying momentum resolution corrections because of two major advantages. First, the MC data must be analyzed only once, and no assumptions about the fit are needed. Secondly, the momentum resolution correction is applied on-the-fly by the fitter, delegating the iterative process to a computer instead of the user.

5.4 Residual Correlations

The purpose of this analysis is study the interaction and scale of the emitting source of the pairs. In order to obtain correct results, it is important for our particle collections to consist of primary particles. In practice, this is difficult to achieve for our Λ and $\bar{\Lambda}$ collections. Many of our Λ particles are not primary, but originate as decay products from other hyperons, including Σ^0, Ξ^-, Ξ^0 and Ω^-. In these decays, the Λ carries away a momentum very similar to that of its parent. As a result, the correlation function between a secondary Λ and, for instance, a K^+ will be sensitive to, and dependent upon, the interaction

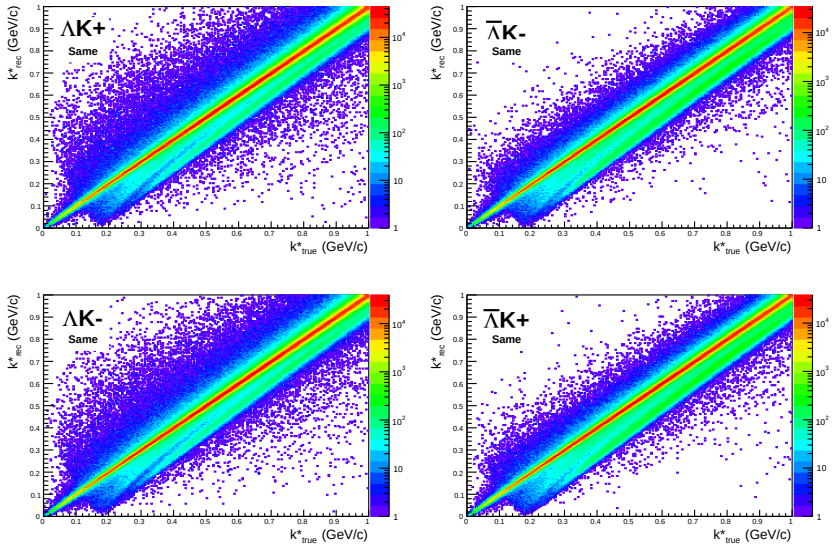

(a) Same Event Pairs ($\Lambda(\bar{\Lambda})K^{\pm}$, 0-10% Centrality)

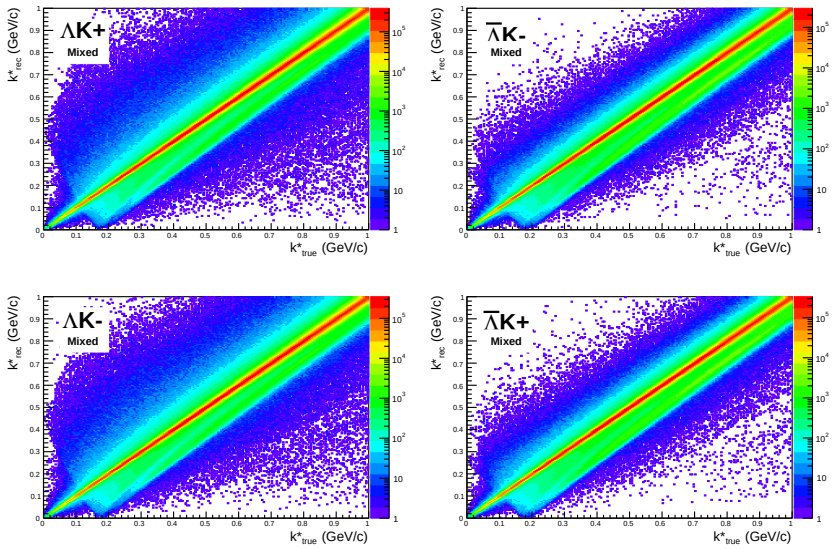

(b) Mixed Event Pairs ($\Lambda(\bar{\Lambda})K^{\pm}$, 0-10% Centrality)

Fig. 16: Sample k^*_{True} vs. k^*_{Rec} plot for $\Lambda(\bar{\Lambda})K^{\pm}$ 0-10% analyses. The structure which appears around $k^*_{Rec} = k^*_{True} - 0.15$ is mainly caused by K^0_S contamination in our $\Lambda(\bar{\Lambda})$ sample. The remaining structure not distributed about $k^*_{Rec} = k^*_{True}$ is due to π and e contamination in our $K^{\pm}$ sample. These contaminations are more clearly visible in Figure 17

between the parent of the Λ and the K^+. In effect, the correlation between the parent of the Λ and the K^+ (ex. Σ^0K^+) will be visible, although smeared out, in the ΛK^+ data. We call this a residual correlation resulting from feed-down.

As it is difficult for us to eliminate these residual correlations in our analyses, we must attempt to account for them in our fitter. To achieve this, we will simultaneously fit the data for both the primary correlation function and the residual correlations. For example, in the simple case of a ΛK^+ analysis with residuals arising soley from Σ^0K^+ feed-down:

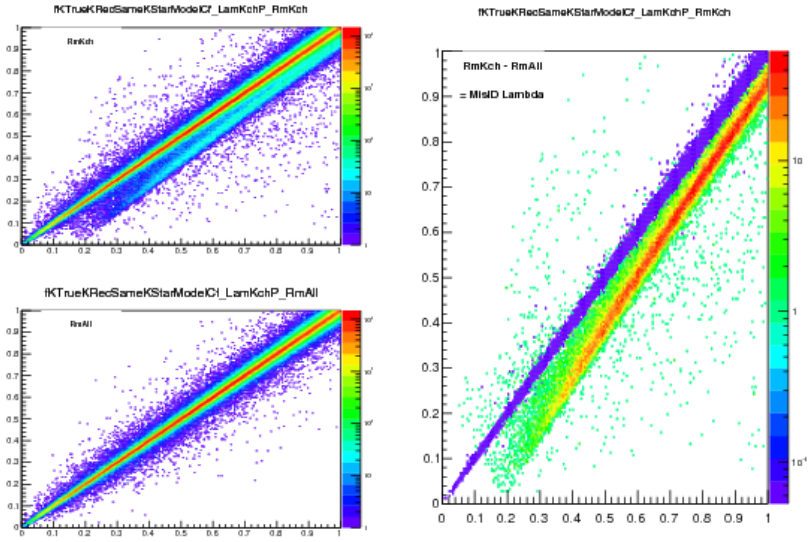

(a) (Top Left) All misidentified K^+ excluded. (Bottom Left) All misidentified Λ and K^+ excluded. (Right) The difference of (Top Left) - (Bottom Left), which reveals the contamination in our Λ collection. The structure which appears around $k^*_{Rec} = k^*_{True} - 0.15$ is mainly caused by K^0_S contamination in our $\Lambda(\bar{\Lambda})$ sample.

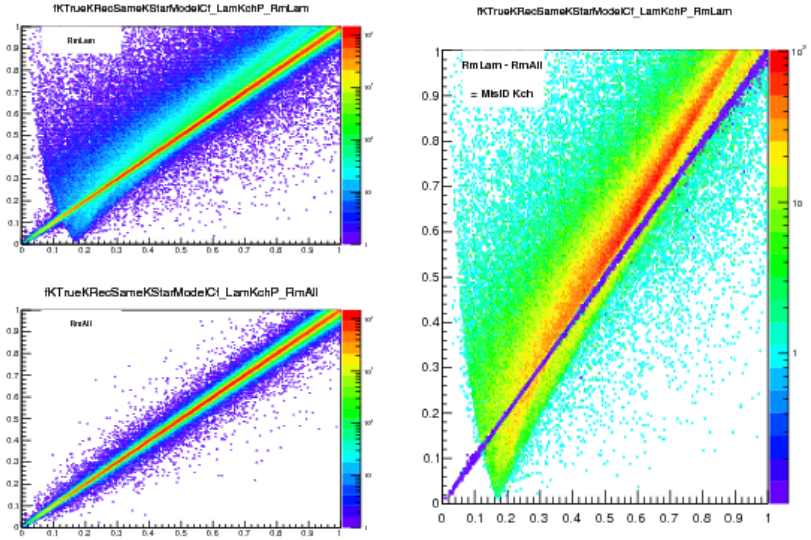

(b) (Top Left) All misidentified Λ excluded. (Bottom Left) All misidentified Λ and K^+ excluded. (Right) The difference of (Top Left) - (Bottom Left), which reveals the contamination in our K^+ collection. The structure not distributed about $k^*_{Rec} = k^*_{True}$ is due to π and e contamination in our K^+ sample.

Fig. 17: Note: This is an old figure and is for a small sample of the data. A new version will be generated shortly. y-axis = k^*_{Rec}, x-axis = k^*_{True}.
(Left) k^*_{Rec} vs. k^*_{True} plots for a small sample of the ΛK^+ 0-10% central analysis, MC truth was used to eliminate misidentified particles in the K^+(a) and Λ(b) collections. (Right) The difference of the top left and bottom left plots. Contaminations in our particle collections are clearly visible. Figure (a) demonstrates a K^0_S contamination in our Λ collection; Figure (b) demonstrates a π and e^- contamination in our $K^\pm$ collection.

$$C_{measured}(k^*_{\Lambda K^+}) = 1 + \lambda_{\Lambda K^+}[C_{\Lambda K^+}(k^*_{\Lambda K^+}) - 1] + \lambda_{\Sigma^0 K^+}[C_{\Sigma^0 K^+}(k^*_{\Lambda K^+}) - 1]$$

$$C_{\Sigma^0 K^+}(k^*_{\Lambda K^+}) \equiv \sum_{k^*_{\Sigma^0 K^+}} \frac{C_{\Sigma^0 K^+}\left(k^*_{\Sigma^0 K^+}\right) T\left(k^*_{\Sigma^0 K^+}, k^*_{\Lambda K^+}\right)}{T\left(k^*_{\Sigma^0 K^+}, k^*_{\Lambda K^+}\right)} \tag{14}$$

$C_{\Sigma^0 K^+}(k^*_{\Sigma^0 K^+})$ is the $\Sigma^0 K^+$ correlation function from, for instance, Equation 4, and T is the transform matrix generated with THERMINATOR. This equation can be easily extended to include feed-down from more sourced:

$$C_{measured}(k^*_{\Lambda K}) = \sum_i \lambda_i C_i(k^*_{\Lambda K}) \tag{15}$$

The framework for extracting the necessary transform matrices from the THERMINATOR data is already in place, and has been used to generate the examples from ΛK^+ and $\bar{\Lambda} K^+$ analyses shown in Figures 18 and 19. However, these residual correlations have not yet been implemented in the fitter.

There is an obvious added complication here, as, for instance, the $\Xi^- K^\pm$ residuals necessitate the inclusion of the CoulombFitter into the process. The complication of combining the two fitters is not as troubling as the increase in fitting time that this is sure to bring. Additionally, in the future, we may combine our ΛK and ΞK analyses to be fit simultaneously.

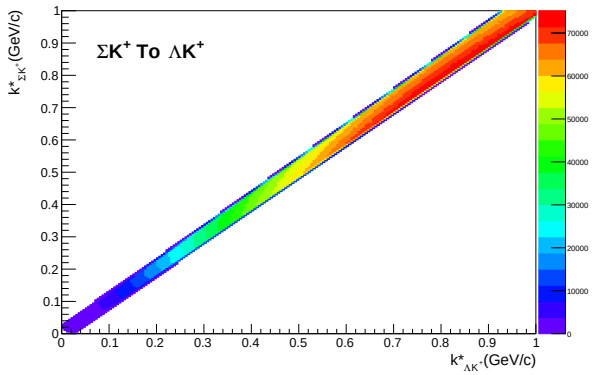

(a) Transform matrix for ΣK^+ pairs into ΛK^+

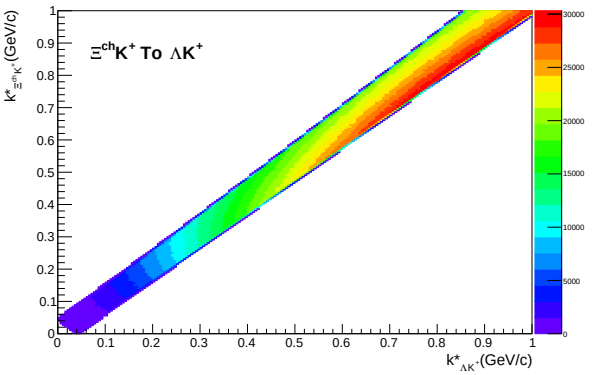

(b) Transform matrix for $\Xi^- K^+$ pairs into ΛK^+

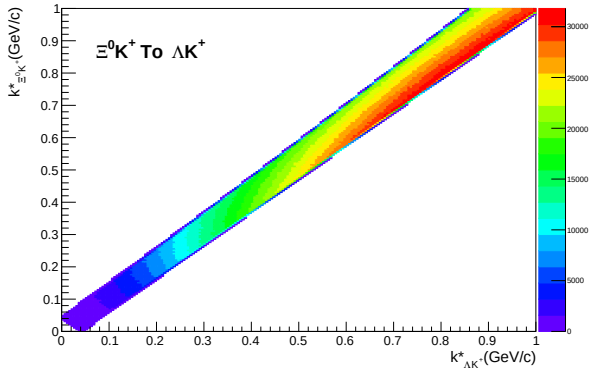

(c) Transform matrix for $\Xi^0 K^+$ pairs into ΛK^+

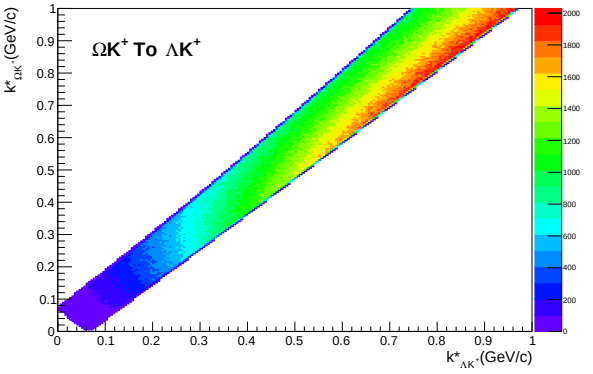

(d) Transform matrix for $\Omega^- K^+$ pairs into ΛK^+

Fig. 18: Transform Matrices generated with THERMINATOR for ΛK^+ Analysis

6 Systematic Errors

This study is currently ongoing, and an estimate of my systematic uncertainties should be complete before 9 December 2016.

In order to understand my systematic uncertainties, the analysis code was run many times using slightly different values for a number of important cuts, and the results were compared. To quantify the effect,

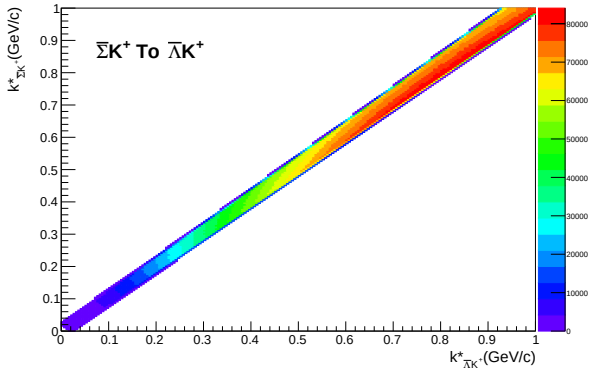

(a) Transform matrix for $\bar{\Sigma}K^+$ pairs into $\bar{\Lambda}K^+$

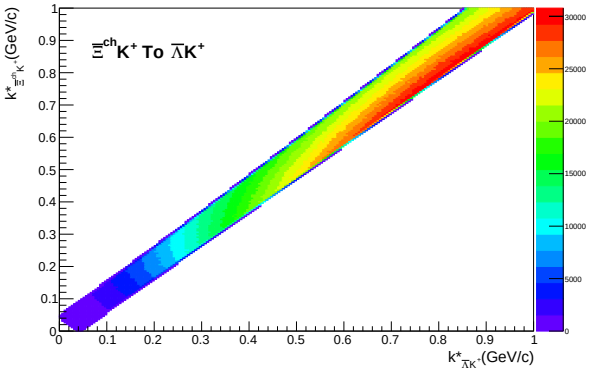

(b) Transform matrix for $\bar{\Xi}^+K^+$ pairs into $\bar{\Lambda}K^+$

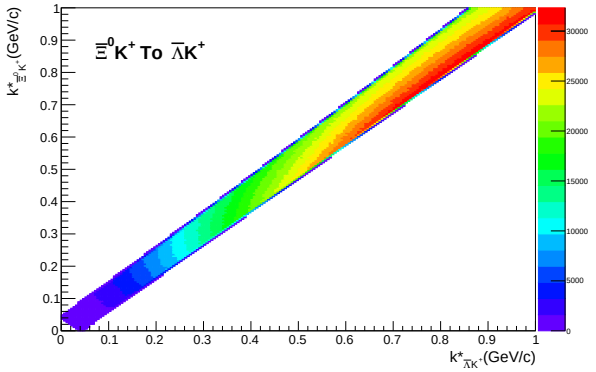

(c) Transform matrix for $\bar{\Xi}^0K^+$ pairs into $\bar{\Lambda}K^+$

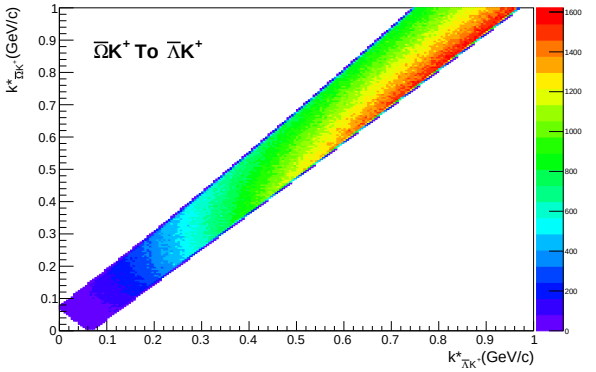

(d) Transform matrix for $\bar{\Omega}^+K^+$ pairs into $\bar{\Lambda}K^+$

Fig. 19: Transform Matrices generated with THERMINATOR for $\bar{\Lambda}K^+$ Analysis

the difference in two correlation functions obtained using different values for a given cut was fit with a simple exponential decay function:

$$\Delta C(k^*) = Ae^{-Bk^*} \tag{16}$$

The amplitude, A, and its associated uncertainty for the various cuts can be found in Tables 1 through 17. The systematic effect of the variation is marked as significant ("Sig" column) if the amplitude is not withih 2σ of 0. Although this proves qualitatively useful, these fits will likely not be used to quantify the systematic effects.

In order to quantify the systematic errors on the correlation functions, all correlations will be averaged, and the resulting variance will be taken as the systematic error. Similarly, the fit parameters extracted from all of these correlation functions will be averaged, and they resulting variances will be taken as the systematic errors for the fit parameters.

6.1 Systematic Errors: ΛK^0_S

6.1.1 Particle and Pair Cuts

The cuts included in the systematic study, as well as the values used in the variations, are listed below. Note, the central value corresponds to that used in the analysis.

1. DCA $\Lambda(\bar{\Lambda})$: $\{4, 5, 6$ mm$\}$

DCA $\Lambda(\bar{\Lambda})$

Pair Type	Centrality	Fit Amplitudes					
		Amplitude	Error	Sig	Amplitude	Error	Sig
		4 vs 5 mm			5 vs 6 mm		
ΛK^0_S	0-10%	2.616e-04	2.840e-04	No	-5.282e-03	4.887e-03	No
	10-30%	-1.236e-03	1.568e-03	No	6.110e-05	1.457e-04	No
	30-50%	-4.664e-02	3.295e-02	No	-1.877e-01	7.037e-02	Yes
$\bar{\Lambda}K^0_S$	0-10%	-6.093e-05	3.827e-05	No	-9.599e-02	1.133e-01	No
	10-30%	-3.478e-05	1.983e-04	No	-2.846e-04	6.743e-04	No
	30-50%	-2.054e-02	2.609e-02	No	-3.701e-03	3.136e-03	No

Table 1: $\Lambda(\bar{\Lambda})K^0_S$ Analyses: DCA $\Lambda(\bar{\Lambda})$ caption

DCA K^0_S

Pair Type	Centrality	Fit Amplitudes					
		Amplitude	Error	Sig	Amplitude	Error	Sig
		2 vs 3 mm			3 vs 4 mm		
ΛK^0_S	0-10%	-1.149e-04	1.616e-04	No	1.495e-04	3.020e-04	No
	10-30%	2.336e-04	7.234e-05	Yes	-2.560e-03	2.270e-03	No
	30-50%	-7.966e-03	4.151e-03	No	-1.721e-02	6.245e-03	Yes
$\bar{\Lambda}K^0_S$	0-10%	6.657e-05	5.808e-04	No	7.037e-05	2.753e-05	Yes
	10-30%	-4.373e-04	3.529e-04	No	-4.653e-04	3.627e-04	No
	30-50%	-2.048e-03	1.296e-03	No	-2.871e-04	8.150e-04	No

Table 2: $\Lambda(\bar{\Lambda})K^0_S$ Analyses: DCA K^0_S caption

2. DCA K^0_S: {2, 3, 4 mm}

3. DCA $\Lambda(\bar{\Lambda})$ Daughters: {3, 4, 5 mm}

4. DCA K^0_S Daughters: {2, 3, 4 mm}

5. $\Lambda(\bar{\Lambda})$ Cosine of Pointing Angle: {0.9992, 0.9993, 0.9994}

6. K^0_S Cosine of Pointing Angle: {0.9992, 0.9993, 0.9994}

7. DCA to Primary Vertex of $p(\bar{p})$ Daughter of $\Lambda(\bar{\Lambda})$: {0.5, 1, 2 mm}

8. DCA to Primary Vertex of $\pi^-(\pi^+)$ Daughter of $\Lambda(\bar{\Lambda})$: {0.5, 1, 2 mm}

9. DCA to Primary Vertex of π^+ Daughter of K^0_S: {2, 3, 4 mm}

10. DCA to Primary Vertex of π^- Daughter of K^0_S: {2, 3, 4 mm}

11. Average Separation of Like-Charge Daughters: {5, 6, 7 cm}

DCA $\Lambda(\bar{\Lambda})$ Daughters

Pair Type	Centrality	Fit Amplitudes					
		Amplitude	Error	Sig	Amplitude	Error	Sig
		3 vs 4 mm			4 vs 5 mm		
ΛK^0_S	0-10%	1.743e-05	3.776e-05	No	1.972e-04	2.813e-04	No
	10-30%	1.293e-04	7.761e-05	No	-8.925e-05	6.165e-05	No
	30-50%	-8.647e-02	9.120e-02	No	-5.097e-02	5.611e-02	No
$\bar{\Lambda}K^0_S$	0-10%	-8.539e-06	3.914e-05	No	5.936e-05	3.128e-05	No
	10-30%	1.001e-04	7.999e-05	No	-2.452e-04	2.952e-04	No
	30-50%	4.672e-05	1.859e-04	No	-1.423e-01	1.753e-01	No

Table 3: $\Lambda(\bar{\Lambda})K^0_S$ Analyses: DCA $\Lambda(\bar{\Lambda})$ Daughters

DCA K^0_S Daughters

Pair Type	Centrality	Fit Amplitudes					
		Amplitude	Error	Sig	Amplitude	Error	Sig
		2 vs 3 mm			3 vs 4 mm		
ΛK^0_S	0-10%	-1.383e-03	1.201e-03	No	-2.394e-03	2.528e-03	No
	10-30%	-1.199e-01	6.112e-02	No	-1.673e-03	1.620e-03	No
	30-50%	-1.397e-01	5.508e-02	Yes	-2.249e-03	3.303e-03	No
$\bar{\Lambda}K^0_S$	0-10%	-3.646e-03	2.561e-03	No	-4.246e-04	5.171e-04	No
	10-30%	1.800e-04	8.734e-05	Yes	-7.128e-04	9.398e-04	No
	30-50%	-2.813e-02	1.883e-02	No	-1.285e-02	9.463e-03	No

Table 4: $\Lambda(\bar{\Lambda})K^0_S$ Analyses: DCA K^0_S Daughters

$\Lambda(\bar{\Lambda})$ Cosine of Pointing Angle

Pair Type	Centrality	Fit Amplitudes					
		Amplitude	Error	Sig	Amplitude	Error	Sig
		0.9992 vs 0.9993			0.9993 vs 0.9994		
ΛK^0_S	0-10%	4.733e-03	2.311e-03	Yes	-7.459e-05	1.768e-04	No
	10-30%	5.201e-03	2.270e-03	Yes	-2.253e-05	7.593e-05	No
	30-50%	-6.078e-05	6.309e-05	No	5.494e-03	1.496e-03	Yes
$\bar{\Lambda}K^0_S$	0-10%	-2.031e-05	8.438e-07	Yes	-4.978e-05	6.433e-05	No
	10-30%	3.929e-04	2.778e-04	No	1.333e-04	2.362e-04	No
	30-50%	1.770e-03	6.120e-04	Yes	1.169e-04	7.436e-05	No

Table 5: $\Lambda(\bar{\Lambda})K^0_S$ Analyses: $\Lambda(\bar{\Lambda})$ Cosine of Pointing Angle

K^0_S Cosine of Pointing Angle

Pair Type	Centrality	Fit Amplitudes					
		Amplitude	Error	Sig	Amplitude	Error	Sig
		0.9992 vs 0.9993			0.9993 vs 0.9994		
ΛK^0_S	0-10%	-3.282e-04	4.102e-04	No	7.088e-04	3.667e-04	No
	10-30%	1.476e-03	2.082e-03	No	8.069e-03	3.961e-03	Yes
	30-50%	-3.150e-04	6.895e-04	No	5.057e-03	2.639e-03	No
$\bar{\Lambda}K^0_S$	0-10%	5.986e-04	4.487e-04	No	7.197e-04	7.865e-04	No
	10-30%	3.562e-03	1.378e-03	Yes	1.303e-03	1.067e-03	No
	30-50%	5.878e-02	8.703e-02	No	1.493e-04	1.017e-04	No

Table 6: $\Lambda(\bar{\Lambda})K^0_S$ Analyses: K^0_S Cosine of Pointing Angle

DCA to Primary Vertex of $p^+(\bar{p}^-)$ Daughter of $\Lambda(\bar{\Lambda})$

Pair Type	Centrality	Fit Amplitudes					
		Amplitude	Error	Sig	Amplitude	Error	Sig
		0.5 vs 1 mm			1 vs 2 mm		
ΛK^0_S	0-10%	0.000e+00	0.000e+00	No	-2.602e-03	2.525e-03	No
	10-30%	2.964e-07	1.165e-06	No	1.702e-04	9.110e-05	No
	30-50%	0.000e+00	0.000e+00	No	5.775e-03	7.524e-03	No
$\bar{\Lambda}K^0_S$	0-10%	0.000e+00	0.000e+00	No	-2.584e-04	4.464e-04	No
	10-30%	0.000e+00	0.000e+00	No	-3.469e-04	1.403e-04	Yes
	30-50%	0.000e+00	0.000e+00	No	-6.689e-04	1.232e-03	No

Table 7: $\Lambda(\bar{\Lambda})K^0_S$ Analyses: DCA to Primary Vertex of $p^+(\bar{p}^-)$ Daughter of $\Lambda(\bar{\Lambda})$

DCA to Primary Vertex of $\pi^-(\pi^+)$ Daughter of $\Lambda(\bar{\Lambda})$

Pair Type	Centrality	Fit Amplitudes					
		Amplitude	Error	Sig	Amplitude	Error	Sig
		2 vs 3 mm			3 vs 4 mm		
ΛK^0_S	0-10%	3.829e-05	1.846e-05	Yes	-4.781e-05	8.826e-05	No
	10-30%	1.498e-03	2.398e-03	No	4.245e+00	4.457e+01	No
	30-50%	3.751e-03	2.567e-03	No	6.001e-03	4.805e-03	No
$\bar{\Lambda}K^0_S$	0-10%	5.680e-05	1.816e-05	Yes	-3.516e-05	2.272e-05	No
	10-30%	1.539e-04	2.857e-04	No	-1.311e-04	4.871e-05	Yes
	30-50%	1.410e-03	1.734e-03	No	4.401e-02	1.349e-02	Yes

Table 8: $\Lambda(\bar{\Lambda})K^0_S$ Analyses: DCA to Primary Vertex of $\pi^-(\pi^+)$ Daughter of $\Lambda(\bar{\Lambda})$

DCA to Primary Vertex of π^+ Daughter of K^0_S

Pair Type	Centrality	Fit Amplitudes					
		Amplitude	Error	Sig	Amplitude	Error	Sig
		2 vs 3 mm			3 vs 4 mm		
ΛK^0_S	0-10%	-4.519e-05	2.636e-05	No	-8.563e-05	3.040e-05	Yes
	10-30%	-8.408e-03	7.107e-03	No	-4.274e-04	9.735e-04	No
	30-50%	2.064e-03	1.619e-03	No	1.274e-03	1.270e-03	No
$\bar{\Lambda}K^0_S$	0-10%	8.474e-04	1.271e-03	No	3.787e-04	3.383e-04	No
	10-30%	-7.583e-05	5.660e-05	No	-7.112e-03	1.605e-02	No
	30-50%	-6.532e-04	1.388e-04	Yes	3.770e-02	1.629e-02	Yes

Table 9: $\Lambda(\bar{\Lambda})K^0_S$ Analyses: DCA to Primary Vertex of π^+ Daughter of K^0_S

DCA to Primary Vertex of π^- Daughter of K^0_S

Pair Type	Centrality	Fit Amplitudes					
		Amplitude	Error	Sig	Amplitude	Error	Sig
		2 vs 3 mm			3 vs 4 mm		
ΛK^0_S	0-10%	-3.283e-04	4.184e-04	No	3.117e-04	2.151e-04	No
	10-30%	-7.208e-07	3.153e-04	No	2.858e-04	6.697e-04	No
	30-50%	4.434e-02	2.574e-02	No	2.761e-04	1.565e-04	No
$\bar{\Lambda}K^0_S$	0-10%	8.823e-05	2.701e-05	Yes	9.286e-02	1.113e-01	No
	10-30%	1.778e-04	5.686e-05	Yes	1.343e-03	1.986e-03	No
	30-50%	1.449e-04	1.368e-04	No	-1.887e-04	1.605e-04	No

Table 10: $\Lambda(\bar{\Lambda})K^0_S$ Analyses: DCA to Primary Vertex of π^- Daughter of K^0_S

Avgerage Separation of Like-Charge Daughters

Pair Type	Daughters		Centrality	Fit Amplitude					
				Amplitude	Error	Sig	Amplitude	Error	Sig
				5.0 vs 6.0 cm			6.0 vs 7.0 cm		
ΛK^0_S	p(Λ)	$\pi^+(K^0_S)$	0-10%	1.665e-05	2.087e-06	Yes	2.653e-04	1.739e-04	No
			10-30%	2.331e-05	4.563e-05	No	-1.713e-05	6.046e-06	Yes
			30-50%	4.333e-04	1.155e-04	Yes	7.198e-04	1.244e-04	Yes
ΛK^0_S	$\pi^-(\Lambda)$	$\pi^-(K^0_S)$	0-10%	7.361e-06	2.047e-06	Yes	-2.548e-05	2.467e-05	No
			10-30%	4.421e-05	3.105e-05	No	7.315e-04	1.322e-04	Yes
			30-50%	6.366e-05	5.813e-05	No	1.154e-04	8.695e-06	Yes
$\bar{\Lambda}K^0_S$	$\pi^+(\bar{\Lambda})$	$\pi^+(K^0_S)$	0-10%	8.888e-04	2.082e-04	Yes	-5.316e-06	3.826e-05	No
			10-30%	9.162e-04	2.614e-04	Yes	1.925e-05	6.041e-05	No
			30-50%	1.478e-04	4.676e-05	Yes	9.973e-05	6.549e-05	No
$\bar{\Lambda}K^0_S$	$\bar{p}^-(\bar{\Lambda})$	$\pi^-(K^0_S)$	0-10%	1.730e-04	1.161e-04	No	-2.798e-05	4.725e-05	No
			10-30%	1.579e-05	5.734e-05	No	-3.884e-07	6.028e-06	No
			30-50%	1.074e-04	3.781e-05	Yes	4.932e-04	2.440e-04	Yes

Table 11: $\Lambda(\bar{\Lambda})K^0_S$ Analyses: Avgerage Separation of Positive Daughters

6.1.2 Non-Flat Background

6.1.3 Fit Range

6.1.4 Normalization Range

6.1.5 Momentum Resolution Correction

6.2 Systematic Errors: $\Lambda K^{\pm}$

6.2.1 Particle and Pair Cuts

The cuts included in the systematic study, as well as the values used in the variations, are listed below. Note, the central value corresponds to that used in the analysis.

1. DCA $\Lambda(\bar{\Lambda})$: {4, 5, 6 mm}
2. DCA $\Lambda(\bar{\Lambda})$ Daughters: {3, 4, 5 mm}
3. $\Lambda(\bar{\Lambda})$ Cosine of Pointing Angle: {0.9992, 0.9993, 0.9994}
4. DCA to Primary Vertex of $p(\bar{p})$ Daughter of $\Lambda(\bar{\Lambda})$: {0.5, 1, 2 mm}
5. DCA to Primary Vertex of $\pi^-(\pi^+)$ Daughter of $\Lambda(\bar{\Lambda})$: {0.5, 1, 2 mm}
6. Average Separation of $\Lambda(\bar{\Lambda})$ Daughter with Same Charge as $K^{\pm}$: {7, 8, 9 cm}

DCA $\Lambda(\bar{\Lambda})$

Pair Type	Centrality	Fit Amplitudes					
		Amplitude	Error	Sig	Amplitude	Error	Sig
		4 vs 5 mm			5 vs 6 mm		
ΛK^+	0-10%	-1.200e-04	8.688e-05	No	2.534e-04	1.983e-04	No
	10-30%	-3.714e-05	1.986e-04	No	6.806e-02	7.932e-02	No
	30-50%	-5.383e-02	6.237e-02	No	-3.545e-04	4.265e-04	No
$\bar{\Lambda}K^-$	0-10%	-1.388e-04	1.057e-04	No	4.615e-05	1.693e-05	Yes
	10-30%	-7.745e-04	4.039e-04	No	-3.957e-05	5.462e-04	No
	30-50%	1.601e-03	1.398e-03	No	2.435e-04	1.118e-03	No
ΛK^-	0-10%	-6.034e-05	1.158e-04	No	1.924e-03	1.398e-03	No
	10-30%	4.468e-05	4.450e-05	No	-4.520e-04	3.092e-04	No
	30-50%	-1.496e-03	9.168e-04	No	-7.476e-04	1.012e-03	No
$\bar{\Lambda}K^+$	0-10%	-1.777e-04	2.999e-04	No	-2.152e-05	1.639e-05	No
	10-30%	-3.655e-04	3.734e-04	No	-8.857e-04	7.247e-04	No
	30-50%	-1.650e-03	1.124e-03	No	-3.706e-04	3.366e-04	No

Table 12: $\Lambda(\bar{\Lambda})K^{\pm}$ Analyses: DCA $\Lambda(\bar{\Lambda})$

DCA $\Lambda(\bar{\Lambda})$ Daughters

Pair Type	Centrality	Fit Amplitudes					
		Amplitude	Error	Sig	Amplitude	Error	Sig
		3 vs 4 mm			4 vs 5 mm		
ΛK^+	0-10%	-1.170e-02	9.437e-03	No	-2.349e-03	1.142e-03	Yes
	10-30%	-3.522e-04	3.863e-04	No	1.359e-05	3.543e-05	No
	30-50%	1.090e-03	1.354e-03	No	-7.623e-02	3.708e-02	Yes
$\bar{\Lambda}K^-$	0-10%	-1.306e-04	1.486e-04	No	-4.771e-04	5.081e-04	No
	10-30%	7.482e-04	8.811e-04	No	8.166e-05	3.779e-05	Yes
	30-50%	-7.928e-04	1.146e-03	No	-2.568e-04	8.664e-05	Yes
ΛK^-	0-10%	-1.498e-04	1.562e-04	No	-5.849e-04	6.665e-04	No
	10-30%	1.204e-05	2.583e-04	No	-9.794e-05	1.314e-04	No
	30-50%	-9.314e-03	6.614e-03	No	-1.264e-04	8.487e-05	No
$\bar{\Lambda}K^+$	0-10%	-4.149e-04	3.296e-04	No	5.288e-05	7.505e-05	No
	10-30%	2.293e-04	3.396e-04	No	-8.853e-04	1.196e-03	No
	30-50%	-6.129e-05	7.969e-04	No	1.735e-04	8.784e-05	No

Table 13: $\Lambda(\bar{\Lambda})K^{\pm}$ Analyses: DCA $\Lambda(\bar{\Lambda})$ Daughters

$\Lambda(\bar{\Lambda})$ Cosine of Pointing Angle

Pair Type	Centrality	Fit Amplitudes					
		Amplitude	Error	Sig	Amplitude	Error	Sig
		0.9992 vs 0.9993			0.9993 vs 0.9994		
ΛK^+	0-10%	-1.448e-05	9.361e-06	No	6.215e-04	4.967e-04	No
	10-30%	3.355e-02	2.063e-02	No	5.291e-04	7.270e-04	No
	30-50%	4.609e-03	5.410e-03	No	1.360e-04	4.949e-05	Yes
$\bar{\Lambda}K^-$	0-10%	-4.085e-06	1.016e-05	No	1.211e-05	1.145e-05	No
	10-30%	1.249e-04	1.660e-04	No	-2.328e-05	2.350e-05	No
	30-50%	2.214e-03	1.301e-03	No	-3.532e-03	4.294e-03	No
ΛK^-	0-10%	3.409e-05	9.589e-06	Yes	1.170e-04	1.430e-04	No
	10-30%	6.537e-05	1.967e-05	Yes	2.119e-04	2.609e-04	No
	30-50%	-4.434e-05	4.608e-05	No	9.610e-05	5.145e-05	No
$\bar{\Lambda}K^+$	0-10%	-3.270e-05	5.714e-05	No	-1.744e-05	1.103e-05	No
	10-30%	-7.203e-05	2.042e-05	Yes	1.023e-04	1.924e-04	No
	30-50%	2.030e-03	1.831e-03	No	7.645e-05	5.303e-05	No

Table 14: $\Lambda(\bar{\Lambda})K^{\pm}$ Analyses: $\Lambda(\bar{\Lambda})$ Cosine of Pointing Angle

DCA to Primary Vertex of $p^+(\bar{p}^-)$ Daughter of $\Lambda(\bar{\Lambda})$

Pair Type	Centrality	Fit Amplitudes					
		Amplitude	Error	Sig	Amplitude	Error	Sig
		0.5 vs 1 mm			1 vs 2 mm		
ΛK^+	0-10%	0.000e+00	0.000e+00	No	-2.429e-04	2.561e-04	No
	10-30%	-3.554e-08	6.097e-08	No	1.598e-04	7.738e-05	Yes
	30-50%	0.000e+00	0.000e+00	No	-2.317e-03	1.992e-03	No
$\bar{\Lambda}K^-$	0-10%	0.000e+00	0.000e+00	No	-9.883e-04	9.265e-04	No
	10-30%	0.000e+00	0.000e+00	No	-2.472e-04	5.419e-04	No
	30-50%	0.000e+00	0.000e+00	No	1.227e-03	1.328e-03	No
ΛK^-	0-10%	0.000e+00	0.000e+00	No	3.677e-03	4.028e-03	No
	10-30%	1.875e-07	1.095e-06	No	6.518e-03	5.373e-03	No
	30-50%	0.000e+00	0.000e+00	No	-2.985e-04	5.747e-04	No
$\bar{\Lambda}K^+$	0-10%	0.000e+00	0.000e+00	No	-4.252e-04	3.414e-04	No
	10-30%	0.000e+00	0.000e+00	No	1.033e-03	8.146e-04	No
	30-50%	0.000e+00	0.000e+00	No	-7.193e-04	7.376e-04	No

Table 15: $\Lambda(\bar{\Lambda})K^{\pm}$ Analyses: DCA to Primary Vertex of $p^+(\bar{p}^-)$ Daughter of $\Lambda(\bar{\Lambda})$

DCA to Primary Vertex of $\pi^-(\pi^+)$ Daughter of $\Lambda(\bar{\Lambda})$

Pair Type	Centrality	Fit Amplitudes					
		Amplitude	Error	Sig	Amplitude	Error	Sig
		2 vs 3 mm			3 vs 4 mm		
ΛK^+	0-10%	7.991e-02	3.641e-01	No	-2.774e-03	3.759e-03	No
	10-30%	-2.559e-05	5.097e-05	No	-4.152e-03	3.267e-03	No
	30-50%	1.461e-02	5.067e-03	Yes	-8.144e-05	3.055e-04	No
$\bar{\Lambda}K^-$	0-10%	-9.069e-06	1.070e-05	No	-1.506e-04	2.900e-04	No
	10-30%	1.485e-05	2.273e-05	No	-2.281e-04	2.219e-04	No
	30-50%	3.830e-03	2.477e-03	No	-2.258e-04	8.241e-04	No
ΛK^-	0-10%	-4.017e-05	5.473e-05	No	-3.418e-05	5.661e-05	No
	10-30%	6.474e-05	7.444e-05	No	4.487e-04	6.332e-04	No
	30-50%	3.344e-03	3.224e-03	No	9.751e-05	7.055e-05	No
$\bar{\Lambda}K^+$	0-10%	2.080e-05	1.035e-05	Yes	-1.947e-05	9.814e-05	No
	10-30%	-4.528e-04	3.642e-04	No	6.138e-05	2.809e-05	Yes
	30-50%	2.643e-04	5.272e-05	Yes	-2.107e-03	1.815e-03	No

Table 16: $\Lambda(\bar{\Lambda})K^{\pm}$ Analyses: DCA to Primary Vertex of $\pi^-(\pi^+)$ Daughter of $\Lambda(\bar{\Lambda})$

Average Separation of $\Lambda(\bar{\Lambda})$ Daughter With Same Charge as $K^{\pm}$

Pair Type	Daughter	Track	Centrality	Fit Amplitudes					
				Amplitude	Error	Sig	Amplitude	Error	Sig
				7 vs 8 mm			8 vs 9 mm		
ΛK^+	$p(\Lambda)$	K^+	0-10%	1.310e-06	1.696e-07	Yes	4.374e-06	2.246e-07	Yes
			10-30%	2.084e-06	4.698e-07	Yes	4.124e-06	4.593e-06	No
			30-50%	-1.186e-03	9.739e-04	No	3.110e-05	3.395e-05	No
$\bar{\Lambda}K^-$	$\bar{p}^-(\bar{\Lambda})$	K^-	0-10%	2.057e-06	1.499e-07	Yes	3.829e-06	1.327e-07	Yes
			10-30%	7.002e-06	6.292e-06	No	4.608e-06	4.256e-06	No
			30-50%	4.608e-06	4.256e-06	No	9.199e-05	7.119e-05	No
ΛK^-	$\pi^-(\Lambda)$	K^-	0-10%	4.686e-06	3.491e-07	Yes	2.311e-06	5.498e-07	Yes
			10-30%	5.411e-06	7.471e-07	Yes	7.344e-06	5.583e-07	Yes
			30-50%	2.045e-04	1.593e-04	No	1.570e-04	3.330e-04	No
$\bar{\Lambda}K^+$	$\pi^+(\bar{\Lambda})$	K^+	0-10%	-3.063e-04	1.137e-04	Yes	-6.134e-05	6.307e-05	No
			10-30%	6.019e-06	6.879e-07	Yes	1.473e-06	1.292e-06	No
			30-50%	1.773e-04	6.857e-05	Yes	1.701e-04	1.120e-04	No

Table 17: $\Lambda(\bar{\Lambda})K^0_S$ Analyses: Average Separation of $\Lambda(\bar{\Lambda})$ Daughter With Same Charge as $K^{\pm}$

References

[1] R. Lednicky and V. L. Lyuboshitz. *Sov. J. Nucl. Phys.*, 35:770, 1982.

[2] Michael Annan Lisa, Scott Pratt, Ron Soltz, and Urs Wiedemann. Femtoscopy in relativistic heavy ion collisions. *Ann. Rev. Nucl. Part. Sci.*, 55:357–402, 2005.

[3] Richard Lednicky. Finite-size effects on two-particle production in continuous and discrete spectrum. *Phys. Part. Nucl.*, 40:307–352, 2009.